



CHALMERS
UNIVERSITY OF TECHNOLOGY

Semiconductor nanocrystals-based triplet-triplet annihilation photon-upconversion: Mechanism, materials and applications

Downloaded from: <https://research.chalmers.se>, 2025-06-15 01:34 UTC

Citation for the original published paper (version of record):

Chen, K., Luan, Q., Liu, T. et al (2025). Semiconductor nanocrystals-based triplet-triplet annihilation photon-upconversion: Mechanism, materials and applications. *Responsive Materials*, 3(1). <http://dx.doi.org/10.1002/rpm.20240030>

N.B. When citing this work, cite the original published paper.

Semiconductor nanocrystals-based triplet-triplet annihilation photon-upconversion: Mechanism, materials and applications

Kezhou Chen^{1,2} | Qingxin Luan^{1,2}  | Tiegen Liu^{1,2} | Bo Albinsson³ | Lili Hou^{1,2} 

¹State Key Laboratory of Precision Measurement Technology and Instruments, Tianjin University, Tianjin, China

²School of Precision Instruments and Optoelectronics Engineering, Tianjin University, Tianjin, China

³Department of Chemistry and Chemical Engineering, Chalmers University of Technology, Gothenburg, Sweden

Correspondence

Tiegen Liu, Bo Albinsson and Lili Hou.
 Email: tgliu@tju.edu.cn, balb@chalmers.se and lilihou@tju.edu.cn

Abstract

Triplet-triplet annihilation photon upconversion (TTA-UC) has emerged as a promising strategy for enhancing solar energy harvesting efficiency by converting two low-energy, long-wavelength photons into a high-energy, short-wavelength photon. In recent years, semiconductor nanocrystals have gained significant attention as efficient photosensitizers for TTA-UC due to their excellent triplet energy transfer efficiency and the ability to tune their bandgap across the solar spectrum. This review focuses on the mechanism of NC-based TTA-UC, emphasizing key parameters to evaluate the performance of TTA-UC systems. The influence of various material-related factors on the overall NC-based TTA-UC performance is thoroughly discussed. Moreover, recent advances in solid-state approaches for NC-based TTA-UC are highlighted, along with an overview of the current status of applications in this field. Lastly, this review identifies the challenges and opportunities that lie ahead in the future development of NC-based TTA-UC, providing insights into the potential advancements and directions for further research.

Keywords

semiconductor nanocrystals, solar energy harvesting, triplet energy transfer, triplet-triplet annihilation photon upconversion

1 | INTRODUCTION

Solar energy, as an abundant, inexhaustible, and clean resource, provides a sustainable solution to reduce energy dependence on fossil fuels and mitigates the harmful effects of global warming.^[1-3] Solar energy has been extensively harnessed to generate electricity,^[4-5] thermal energy,^[6-7] architecture integrated photovoltaics,^[8] as well as for photocatalysis^[9] such as water splitting^[10-11] and CO₂ reduction.^[12-13] The spectrum of the sun at the Earth's surface is spread across ultraviolet (UV), the visible and near-infrared (NIR) ranges,^[8] as shown in Figure 1. Under ideal circumstances, sunlight can reach the surface of the Earth with an irradiation of about 1000 W/m².^[14] However, because of the mismatch of the solar spectrum and bandgaps of common

light harvesting materials such as silicon (1.1 eV), a considerable portion of the sunlight's energy is not effectively utilized by solar cells, as indicated in Figure 1. The photons with energies higher than bandgap of solar cell materials (UV light and high-energy visible light) carry excess energy that is not easily converted. Similarly, photons with lower energies (NIR light) do not possess enough energy to overcome the bandgap, so they are not converted either. According to the Shockley-Queisser limit,^[15] the maximum solar conversion efficiency is limited to 33% for a single-junction solar cell.^[16]

Photon upconversion is a process that has the potential to be applied to enhance the performance of solar energy harvesting by converting low-energy photons into high-energy photons.^[17-19] Although surpassing the Shockley-Queisser limit for solar energy conversion has not been practically

This is an open access article under the terms of the [Creative Commons Attribution](https://creativecommons.org/licenses/by/4.0/) License, which permits use, distribution and reproduction in any medium, provided the original work is properly cited.

© 2024 The Author(s). *Responsive Materials* published by John Wiley & Sons Australia, Ltd on behalf of Southeast University.

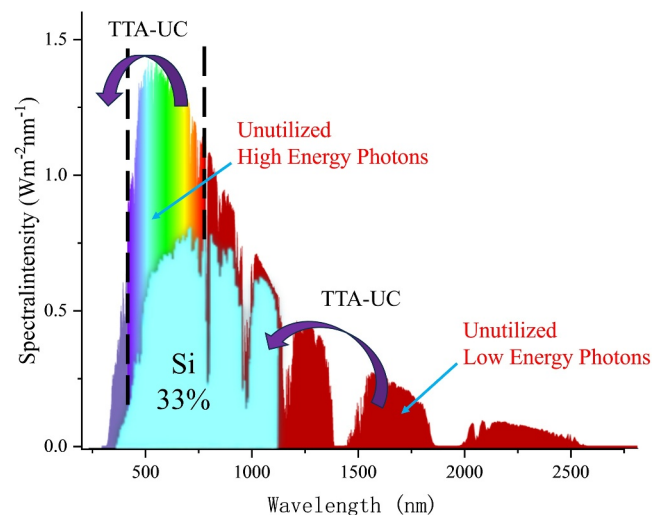


FIGURE 1 Solar spectrum and silicon-based solar cell loss channels, which can be mitigated by the triplet-triplet annihilation photon upconversion (TTA-UC) process through converting near-infrared (NIR) to visible light and enabling photocatalysis through upconversion of visible to ultraviolet (UV) light.

achieved,^[20] the upconversion process can theoretically enhance the efficiency of solar cells imposed by the spectral mismatch between the solar spectrum and the bandgap of solar cell materials, which enables absorption of NIR photons to be upconverted to visible photons.^[21] Additionally, the upconversion of abundant visible light photons to high-energy UV light can enhance efficiency in photocatalytic applications.^[22] Compared to nonlinear optics upconversion^[23-24] and rare earth-doped nanoparticle upconversion,^[25-26] triplet-triplet annihilation photon upconversion (TTA-UC) exhibits high upconversion efficiency for non-coherent light and low operating light intensity (at solar-level irradiation). This makes TTA-UC suitable for practical applications in solar energy harvesting,^[27-30] as well as in biological applications,^[31-32] optoelectronic devices^[33] and additive manufacturing.^[34-35] Many studies of TTA-UC commonly use metal complexes as photosensitizers, such as Ru complexes,^[36] Pt or Pd porphyrin/phthalocyanine complexes,^[37-38] facilitated by their strong spin-orbit coupling. However, the conventional application of these sensitizers for TTA-UC faces limitations due to their restricted molecular design, comparatively low light absorption, and large singlet-triplet splitting, thus limiting the upconverted spectral range.^[39]

Semiconductor nanocrystals (NCs), also known as quantum dots (QDs), are nanometer-sized clusters or crystals consisting of few hundreds to a few thousands of atoms with the quantum confinement in three dimensions.^[40-41] Due to the restricted density of states, NCs exhibit size-dependent electronic transitions, with the energy gap between the highest occupied state (valence band) and the lowest unoccupied state (conduction band) becoming larger as the crystal size decreases. Consequently, the optical absorption and emission characteristics of QDs can be tuned by

controlling their size.^[42] The unique characteristics of QDs, such as their size-tunable optical properties, high absorption cross sections, bright photoluminescence (PL), make them widely applied in lighting^[43-44] and display,^[45] optoelectronics,^[46-47] solar cells,^[48-49] and bioimaging and detection.^[50-51] Over the past decade, NCs have emerged as a promising class of photosensitizer materials^[52-55] and have found increased applications in TTA-UC. This is primarily attributed to the small splitting of singlet-like and triplet-like state and the capability in efficiently sensitizing molecular triplets.^[56-60] Additionally, the size of the NCs can be adjusted to match the incident light wavelength and thereby to enhance the efficiency of TTA-UC.

Encouraged by the rapid progress of NC-based TTA-UC, this review aims to provide an in-depth exploration of the mechanism, materials, and applications of this new class of TTA-UC. This review provides a concise description of the NC-based TTA-UC process and discusses key parameters for evaluating upconversion performance. Here we focus on two typical NCs, metal chalcogenides and perovskite NCs, examining how size, surfactant ligands, shape, quality, and core/shell structure impact TTA-UC performance. We also delve into the materials used as mediators, analyzing their anchoring groups, numbers, bridge distances, and orientations in relation to energy transfer and impact on TTA-UC performance. We highlight the updated solid-state approaches of NC-based TTA-UC, followed by the recent applications of NC-based TTA-UC in solar energy harvesting and photochemistry. There are recent reviews on TTA-UC from different aspects, such as spectral regions,^[61-62] organic material,^[63-64] applications.^[65-66] In this review with a focus on NC sensitized TTA-UC, we have provided a detailed investigation in the spectroscopy, mechanisms, NCs' size and shape, mediator alignment, anchor groups, and have a comprehensive discussion on solid state approaches and special applications of NC-based TTA-UC materials. The aim of this review is to serve as a comprehensive resource for researchers interested in NC-based TTA-UC, through deepened understanding of the underlying mechanisms of TTA-UC and exploring different NC materials. We hope this review can help to potentially inspire further research and development of NC-based TTA-UC towards solar energy harvesting and other applications.

2 | MECHANISM OF NC-BASED TTA-UC

2.1 | Photophysical processes

NC-based TTA-UC system generally includes three components: NCs, mediators (also referred to as transmitters), and annihilators (also referred to as emitters), as shown in Figure 2. NCs absorb low-energy photons to their excited states which have mixed singlet and triplet character due to the strong spin-orbit coupling of NCs.^[67-71] The excited state lifetime of NCs is generally on the timescale of tens of nanosecond to few microsecond, which is too short for

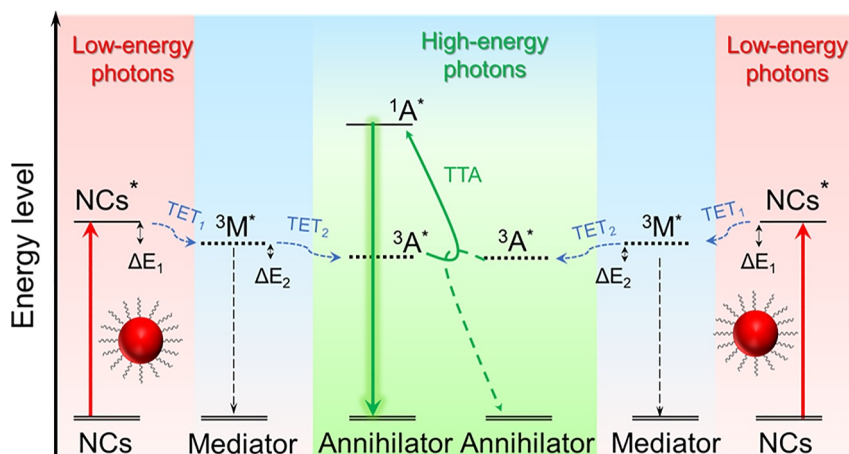


FIGURE 2 The components and mechanism of NC-based triplet-triplet annihilation photon upconversion (TTA-UC). Two low-energy photons are absorbed by the nanocrystals (NCs), followed by a first triplet energy transfer (TET_1) to the mediators ($^3M^*$), which further undergoes a second triplet energy transfer (TET_2) to populate the triplet state of the annihilators ($^3A^*$). Subsequently, two triplet excited annihilators interact and undergo triplet-triplet annihilation (TTA), resulting in the formation of a singlet excited annihilator ($^1A^*$), capable of emitting a high-energy photon.

diffusional sensitization of the triplet state of the annihilator. Therefore, mediators are commonly used to harvest the triplets of NCs by anchoring to the surface; a long-lived mediator triplet (on the timescale of microseconds to milliseconds) can be generated via triplet energy transfer (TET) from the NC to the mediator.^[56,72] The triplet energy of the mediator is then transferred to the annihilator via a second triplet energy transfer (TET_2) process. When two triplet excited annihilators encounter, triplet-triplet annihilation (TTA) can occur to populate one annihilator to its first singlet excited state (S_1), from where high-energy photons can be emitted. We have summarized the commonly used NCs, mediators and annihilators for NC-based TTA-UC in Figure 3, and the detailed properties and performance of these TTA-UC systems are compiled in Table 1.

There are two requirements to achieve NC-based TTA-UC: (a) The first triplet excited state (T_1) of the mediator should be lower than the lowest excited state of the NCs, although endothermic TET from the NCs to the mediators has been reported.^[126-127] Reversible TET leads to slow TET and reduces the efficiency of the overall process. Higher efficiency is generally achieved when the energy gap (ΔE_1) is greater than 0.2 eV; (b) The T_1 state of the annihilator should be equal to or lower in energy than T_1 of the mediator to enable an efficient TET_2 process. Typically, a larger driving force can lead to higher efficiencies in both TET processes, however, this comes at the expense of a smaller upconverted wavelength range (a smaller anti-Stokes shift).

Performance evaluation of the NC-based TTA-UC system relies on a few key parameters, namely photon upconversion quantum yield (UCQY, Φ_{UC}), anti-Stokes wavelength shift, and the excitation intensity threshold (*I_{th}*). In the following discussion, we focus on the merits of these three parameters and corresponding characterization methods of NC-based TTA-NCs.

2.2 | Photon UCQY

The UCQY is defined as the ratio of the number of upconverted high-energy photons to the number of absorbed low-energy photons, as shown in Equation (1):

$$\Phi_{UC} = \frac{\text{the number of emitted high energy photons}}{\text{the number of absorbed low energy photons}} \quad (1)$$

The maximum Φ_{UC} is 50% as one high-energy photon is generated from the interaction of two annihilator triplets. It is important to note that some TTA-UC publications have reported a Φ_{UC} normalized to 100% by multiplying the measured value with a factor of 2. However, it is not recommended to normalize UCQY in this manner, as it deviates from the general definition of quantum yields.^[128] For a detailed discussion on the definitions of UCQY, we recommend references.^[129-131] To ensure clear comparisons, the Φ_{UC} values reported for NC-based TTA-UC systems in Table 1 have been adjusted to non-normalized values. In Equation (1), the UCQY is based on the observation of emitted photons, which can be influenced by the sample architecture, inner filter effects, and scattering. It is worth noting that the upconverted singlet excited states of the annihilators and/or the generated upconverted photons, before being reabsorbed, can also find practical applications in solar energy harvesting and photochemistry.^[17,132-133]

The UCQY of NC-based TTA-UC systems is the product of the efficiencies of each involved sub-step energy transfer processes, as presented in Equation (2):

$$\Phi_{UC} = f\Phi_{TET_1}\Phi_{TET_2}\Phi_{TTA}\Phi_A \quad (2)$$

where, f is a spin statistical factor, indicating the probability that an excited annihilator triplet yields an excited singlet

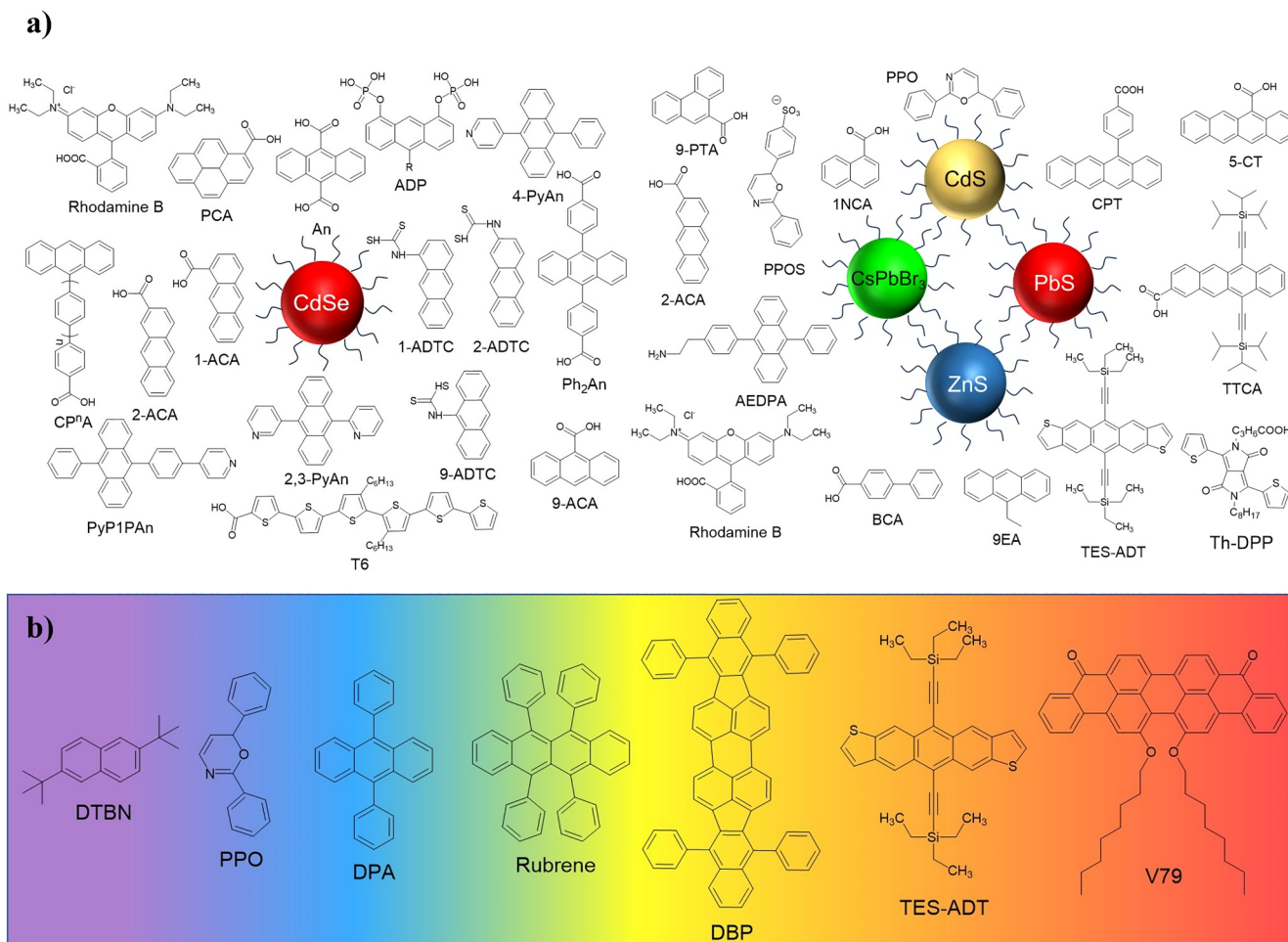


FIGURE 3 Chemical structures of commonly used (a) nanocrystals (NCs) and mediators, (b) annihilators.

following TTA,^[131] Φ_{TET_1} , Φ_{TET_2} , and Φ_{TTA} are the efficiencies of TET₁ from NCs to the mediator, TET₂ from the mediator to the annihilator, and TTA between two annihilators, respectively; Φ_A is the photoluminescence quantum yield (PLQY) of the annihilator. In molecular sensitized TTA-UC system, Equation (2) contains a parameter of Φ_{ISC} , the efficiency of intersystem crossing (ISC). This parameter is lacking because the triplet exciton generation quantum yield of the NCs is nearly unity, which is a result of the strong spin-orbit coupling within heavy metal NCs. This coupling enables the mixing of singlet and triplet spin characters in exciton states. The impact of the above factors and efficiencies on Φ_{UC} will be briefly discussed below, while the detailed impact of the overall TTA-UC performance from materials point of views will be discussed in Section 3.

The spin statistical factor (f) is determined by the precise alignment of S_1 , T_1 , and the second triplet state energies (T_2) of the annihilators.^[134] When $2 \times E(T_1) < E(T_2)$, f could take values above the commonly encountered value of 2/5. In perylene, where this condition is met, the f factor approaches unity due to the inaccessibility of the T_2 state during the TTA process^[135,136]. In rubrene, f is reported to lie around 0.6 in solution, and the creation of T_2 is slightly endothermic during the TTA process and the fast high-level

reverse-ISC allows the transition from T_2 to S_1 , out-competing nonradiative decay from T_2 to T_1 ^[134,137]. When $2 \times E(T_1) > E(T_2)$ in an annihilator species, such as the cases of 9,10-diphenylanthracene (DPA), T_2 state is energetically accessible during the TTA process, f takes the value of 0.4 for strongly exchange-coupled triplet pairs, with the maximum of Φ_{UC} to 20%. Functionalizing DPA to adjust the energy levels and triplet lifetime can prohibit energy loss channels and thus to enhance the Φ_{UC} ^[138,139].

The efficiency of TET₁ from NCs to the mediator (Φ_{TET_1}) depends on the properties of NCs, mediators, and their interface. Sections 3 and 4 will discuss material influences on TET₁. Significant efforts have focused on optimizing the NCs/mediator interface to achieve $\Phi_{TET_1} > 90\%$, long triplet lifetimes, and fast TET rates.^[56,76,114,140] The mechanism of energy transfer at these hybrid interfaces has been reviewed by Tang,^[141] Wu,^[142] Rao,^[143] and Davis.^[57]

In principle, the efficiency of TET₂ of NC-based TTA-UC system from the mediator to the annihilator (Φ_{TET_2}) is not a major concern for systems as the concentration of the annihilator typically is high (>1 mM) in solution, thus yielding a sensitization process with close to unit efficiency.^[144] However, this scenario only applies when the concentration of excited mediators on the NCs' surface is sufficiently high

TABLE 1 Triplet-triplet annihilation photon upconversion (TTA-UC) based on semiconductor nanocrystals (NCs) (quantum dots)^a.

NCs	Mediators	Annihilators	EnT types	I_{th} [mW cm ⁻²]	λ_{ex} [nm]	λ_{em} [nm]	Φ_{UC} [%] ^b	Ref
CdS/ZnS NCs	PPO	PPO	Not reported	7100	405	355	2.6	[73]
CdS NCs	INCA	PPO	Not reported	Not reported	405	355	0.4	
CsPbX ₃ NCs	INCA	PPO	Not reported	4700	445	363	>2	[74]
CsPbBr ₃ NCs	INCA	PPO	Not reported	1900	443	355	5.1	[75]
CdS NCs	3PCA	PPO	Dexter-like	950	405	340–400	10.4	[76]
CsPbBr ₃ NCs	PPOS	TIPS-Nph	Not reported	1600	515	375	0.007	[77]
CsPbBr ₃ NCs	9-PTA	PPO	Endothermic energy transfer	2200	473	355	2.25 ± 0.25	[78]
				1600	443		6.1 ± 0.4	
ZnSe/ZnS NCs	BCA	DTBN	Electron transfer	2400	405	310–380	3.1	[79]
CsPbBr ₃ NPLs	9-PCA	PPO	Not reported	620	450	355	Not reported	[80]
CdSe NCs	9-ACA	DPA	Dexter-like	>10,000	532	432	4.5	[81]
2.7 nmCdSe NCs	9-ACA	DPA	Not reported	19,800	488	400–450	7.5	[82]
				12,700	532		7.7	
CdSe/ZnS NCs	4-PyAn	DPA	Not reported	290	532	433	0.7	[83]
CdSe/ZnS NCs	Not reported			810			0.045	
CdSe NCs	4-PyAn			1290			0.013	
2.6 nm CdSe NCs	9ACA	DPA	Dexter-like	Not reported	532	432	7.15	[84]
	CPA						1.95	
	CPPA						0.2	
CdSe NCs	2,3-PyAn	DPA	Not reported	146.8	532	432	6.05	[85]
CsPbX ₃ (X = Br/I) NCs	AEDPA	DPA	Not reported	25	532	434	0.65	[86]
2.39 nm CdSe NCs	1,2,9-ACA	DPA	Not reported	Not reported	532	Not reported	1.9,0.6, 5.95	[87]
	1,2,9-ADTC				/488		1.5,0.55,0.05	
CdSe NCs	9-ACA	DPA	Not reported	Not reported	488	430	4.65	[88]
CdSe/CdS NCs	Not reported	A-MOF (Ph ₂ An + Zn(II))	Dexter-like	1000	532	450	0.00045	[89]
CuInS ₂ /ZnS NCs	9-ACA	DPA	Not reported	>15,000	520	Not reported	9.3	[90]
CdSe NCs	Not reported	T6	Dexter-like	Not reported	520	Not reported	Not reported	[91]
CdSe NCs	Ph ₂ An	Ph ₂ An	Not reported	Not reported	560	Not reported	0.325	[92]
	An	An						
CsPbX ₃ (Cl/Br) NCs	Rhodamine B	DPA	Electron transfer	700	447	Not reported	3.55	[93]
InP/ZnSe/ZnS NCs	9-ACA	DPA	Not reported	570	530	402	5.0	[94]
CdSe NCs	9-ACA	DPA	Not reported	Not reported	532	430	7.9	[95]
CdSe/ZnS NCs	Rhodamine B	DPA	Electron transfer	1200	635	402	1.4	[96]
CdSe NCs	ADP	DPA	Not reported	163	488	430	8.5	[97]
CdSe: Au NCs	9-ACA	DPA		200	532	425	12	[98]

(Continues)

TABLE 1 (Continued)

NCs	Mediators	Annihilators	EnT types	I_{th} [mW cm ⁻²]	λ_{ex} [nm]	λ_{em} [nm]	Φ_{UC} [%] ^b	Ref
			Hole-routing energy transfer					
CsPbBr ₃ NCs	2-ACA	DPA	Not reported	6900	443	425	6.5	[99]
CdSe NCs	PyPOPAn	DPA	Charge hopping	Not reported	488	430	5.8	[100]
	PyPIPAn						2.25	
CdSe NPL	9-ACA	DPA	Not reported	237	532	430	2.7	[101]
CdTe NR	9-ACA	DPA	Dexter-like	93	520	425	2.15	[102]
Si NCs	9EA	DPA	Not reported	Not reported	532	425	7.5	[103]
CdSe NCs	9-ACA	DPA	Not reported	Not reported	532	430	1.5	[104]
PbS NCs	CPA	DPA	Dexter-like	220	637	430	0.3	[105]
CdSe NCs	Not reported	DPA	Direct energy transfer	Not reported	488	430	3.47	[106]
ZnSe/InP NCs	9-ACA	DPA	Not reported	1200	532	432	4.16	[107]
ZnSe/InP/ZnS NCs				600			4	
PbSe NCs	Not reported	Rubrene	Dexter-like	>100,000	980	568	0.005	[81]
PbS NCs	Not reported	Rubrene: 0.5% DBP	Not reported	12,000	850	612	0.6	[108]
				17,000	960		0.25	
				26,000	1010		0.1	
2.9 nmPbS NCs	CPT	Rubrene	Dexter-like	Not reported	808	570	0.85	[109]
2.5 nmPbSe NCs							1.06	
PbS/CdS NCs	5-CT	Rubrene	Dexter-like	3.2	808	560	4.2	[110]
PbSe NCs	Not reported	Rubrene	Dexter-like	Not reported	808	560	0.005	[111]
PbS NCs	Not reported	Rubrene: 0.5% DBP	Not reported	1100	980	610	0.8	[112]
PbS NCs		Rubrene: 0.5% DBP	Dexter-like	Not reported	808	610	3.5	[113]
2.7 nmPbS NCs	5-CT	Rubrene	Not reported	Not reported	785	560	1.75	[114]
3.2 nmPbS/CdS NCs	5-CT	Rubrene	Not reported	Not reported	785	560	2.5	
PbS-ZnS NCs	Not reported	Rubrene	Dexter-like	Not reported	785	560	0.14	[115]
Pbs-CdS NCs							0.065	
PbS-T NCs	5-CT	Rubrene	Not reported	53,400	781	560	5.9	[116]
PbS-S NCs	5-CT	Rubrene	Not reported	Not reported	781	560	2.3	
MA _{0.15} FA _{0.85} PbI ₃	Not reported	Rubrene (1% DBP)	Hole transfer	500	785	610	1.55	[117]
PbS NCs	TES-ADT	TES-ADT (50 mM)	Dexter-like	43,000	1064	660	0.047	[118]
MAFAPbI ₃	Not reported	Rubrene/1%DBP	Not reported	8.2	780	<650	Not reported	[119]
PbS NCs	5-CT	Rubrene	Dexter-like	Not reported	781	560	5.9	[120]
	5-CPT						2.75	
	5-CPPT						1.25	
PbS NCs	TTCA	V79	Not reported	Not reported	808	650–800	0.031	[121]
PbS NCs	Not reported	Rubrene (0.5–1%DBP)	Not reported	13	980	610	0.03	[122]
PbS NCs	Not reported	TES-ADT	Not reported	>66,000	785	580	0.145	[123]
				>113,000	975		0.03	
CuInSe ₂ (Zn)/ZnS NCs	5-CT	Rubrene	Not reported	2100	808	560	8.35	[124]

TABLE 1 (Continued)

NCs	Mediators	Annihilators	EnT types	I_{th} [mW cm ⁻²]	λ_{ex} [nm]	λ_{em} [nm]	Φ_{UC} [%] ^b	Ref
PbS NCs	Th-DPP	Rubrene	Dexter-like	4800	808	554	6.75	[125]
				23,500	1064	554	0.19	

Abbreviations: ADP, adenosine diphosphate; AEDPA, 2-(4-(10-phenylanthracen-9-yl)phenyl)ethan-1-amine; BCA, bichinchonic acid; CPA, 4-Chlorophenoxyacetic acid; CPPA, 3-Chloroperbenzoic acid; DBP, dibutyl phthalate; DPA, 9,10-diphenylanthracene; DTBN, 5,5'-Dithiobis-(2-nitrobenzoic acid); NPL, nanoplatelet; NR, nanorod; PPO, PPO, 2,5-diphenyloxazole; PPOS, 4-(2-phenyloxazol-5-yl)benzenesulfonate; TES-ADT, 5,11-bis(triethylsilylethynyl)anthradithiophene; TTCA, trithiocyanuric acid.

^aDifferent colors in the table represent different upconversion wavelength regions.

^bThe maximum upconversion quantum yield (Φ_{UC}) is 50%.

coupled with a long triplet lifetime. Recent studies reveal that Φ_{TET_2} scales nonlinearly with changes in Φ_{TET_1} .^[94, 120]

Φ_{TTA} and Φ_A depend on the intrinsic properties of the annihilator, including triplet lifetime, excited state energies, and nonradiative decay rates. Understanding these properties is key to analyzing NC-based TTA-UC systems^[134, 145]. Common annihilators are listed in Figure 3b and detailed in Section 5.

2.3 | Apparent anti-Stokes shift of NC-based TTA-UC

In most TTA-UC publications the anti-Stokes shift is reported to represent the energy difference (in eV or cm⁻¹) between upconverted photons and the excitation photons. According to International Union of Pure and Applied Chemistry standards, a Stokes shift is defined as the energy difference between the absorption and emission peak maxima of the same electronic transition.^[128] However, in TTA-UC processes, the absorption and emission processes do not originate from the same electronic transition, Hanson and co-workers proposed to describe it as an apparent anti-Stokes shift.^[129] To report the value of this apparent anti-Stokes shift, it is crucial to consider the lowest energy absorption peak of the sensitizer and the highest emission peak of the annihilator, rather than solely focusing on the excitation wavelength. As TTA-UC systems can be excited into low-energy absorbance shoulders by using higher-intensity lasers, it can artificially increase the shift, and different values can be obtained for the same system.

For TTA-UC systems based on molecular sensitizers, the ISC process is crucial for accessing molecular excited triplets, and the large singlet-triplet gap (0.1–1 eV)^[146] results in a small apparent anti-Stokes shift.^[18, 147] Achieving a large shift at desired wavelength range is difficult due to the complexities involved in precisely tuning the absorption band and excited state energies of a molecular sensitizer. These challenges arise from the intricacies of chemical synthesis and the difficulties in energy matching with paired annihilators. In contrast, colloidal NCs offer a straightforward approach to adjust size-dependent absorption and excited state energy by controlling the conditions of the colloidal synthesis. The achievement of large apparent anti-Stokes shift in NC-based TTA-UC systems, relies on the small splitting (~20 meV) between bright (singlet-like) and dark (triplet-like) state of the NCs.^[56, 67, 148] Although the

requirement of a mediator in NC-based TTA-UC can lead to some energy loss, rationally designing the interface between NCs and surface-anchored mediators or eliminating the use of a mediator altogether can achieve anti-Stokes shift approaching 1 eV or more.^[76, 81, 108, 118] The excitation wavelength and the upconverted wavelength of NC-based TTA-UC systems are summarized in Table 1.

2.4 | Threshold of NC-based TTA-UC

The I_{th} of TTA-UC systems represent the onset intensity at which the maximum efficiency regime is reached.^[149, 150] When the excitation intensity is below I_{th} , the concentration of annihilator triplets remains low, and their decay primarily follows first-order processes. Consequently, the number of annihilator triplets increases linearly with the excitation power, resulting in quadratic growth of TTA-UC intensity and inefficient upconverted emission. In contrast, when the excitation intensity surpasses I_{th} , the concentration of annihilator triplets becomes sufficiently high for bimolecular TTA to become the dominant decay pathway. As a result, the TTA-UC intensity grows linearly with the excitation power. This threshold is a significant parameter in evaluating TTA-UC systems because it determines the relevance of the upconversion system for practical solar energy harvesting application. The threshold can be determined by measuring and plotting the TTA-UC intensity against the excitation power density on a log-log plot. The quadratic growth can be fitted using a slope of 2 for lower excitation power, while the linear growth can be fitted with a slope of 1 for higher excitation powers. The value of I_{th} corresponds to the power density at the intersection point of these two lines. The threshold of reported NC-based TTA-UC system is summarized in Table 1. It should be noted that although the threshold of NC-based TTA-UC can be reduced by increasing the concentration of NCs to efficiently absorbing incident photons, it also causes stronger reabsorption of the upconversion photons thus lowering the external UCQY.

2.5 | Methods of performance characterization

From the NCs perspective, obtaining insights into key optical properties, such as size distribution, PLQY, and spectral position, requires UV-visible absorption and PL emission

spectroscopies. The absorption wavelength of the NCs can be also used to estimate both the size and excited state energies.^[151-152] The morphology of NCs can be characterized by scanning electron microscopy, transmission electron microscopy, and dynamic light scattering. The number of mediators on the surface of the NCs can be characterized by UV-visible absorption, Fourier-transform infrared (FTIR), Nuclear Magnetic Resonance Spectroscopy, techniques, among others.

The upconverted PL spectra can be recorded by modifying the configuration of a standard spectrofluorometer. This modification involves replacing the excitation light source with an adjustable light source that covers a wide range of power intensities, from $\mu\text{W}/\text{cm}^2$ to W/cm^2 or even higher, depending on the threshold intensity of the TTA-UC system. Investigating the efficiency of each energy transfer step and its impact on the overall UCQY is crucial for NC-based TTA-UC systems. To achieve this, it requires the use of femtosecond and nanosecond transient absorption spectroscopies to analyze the formation of triplet states, the upconversion process, and fast competing processes. Additionally, conventional steady-state PL spectra, time-correlated single-photon counting, and other transient emission techniques are utilized to determine the quenching efficiency.

Obtaining key parameters for TTA-UC performance, particularly threshold determination, can be time-consuming as it requires precise measurement of more than tens of upconverted intensities across a wide range of excitation intensity. Recently, Edhborg and co-workers proposed a relatively easy method by which the rate of TTA, triplet lifetime, and threshold may be determined simultaneously using the same set of time-resolved emission measurements.^[153-154] The system is based on using a pulse generator that triggers a continuous wave diode laser to excite the sample with a square pulse sequence. The subsequent emission is recorded by an oscilloscope. By globally fitting the decay traces, photon upconversion luminescence at various excitation intensity, triplet excited-state lifetimes (τ_T), rate constants for TTA (k_{TTA}), and I_{th} can be determined.

3 | NC MATERIALS FOR TTA-UC

The quality of NCs is key for constructing NC-based TTA-UC system, and the properties of NCs significantly influence TTA-UC performance. This section examines the synthesis methods, size, surfactant ligand length, shape, quality, and core/shell structures of NCs and their impact on TTA-UC. Understanding and optimizing these factors are crucial for enhancing the NC efficiency and the performance of TTA-UC systems.

3.1 | The synthesis of NCs

The most commonly used method of synthesizing NCs is colloidal synthesis.^[155,156] Precursors can react in a colloidal

suspension, and the nucleation and growth of NCs is controlled by surfactant ligands that bind to the surface of NCs. The size and shape of NCs can be controlled by selection of precursors and surfactant ligands, as well as reaction conditions, such as temperature, pressure, and reaction time. Wet colloidal synthesis can produce high-quality NCs with well-controlled size, shape, and composition, which are important properties for many applications including TTA-UC. It should be noted that wet chemistry synthesis of NCs sometime can lead to contamination of NCs due to impurities present in the precursors or solvent. Therefore, it is crucial to carefully purify NCs with proper solvent and centrifugation or filtration to remove any impurities.

Colloidal NCs via wet chemistry synthesis are well-suited for TTA-UC, as it allows precise control of the size and therefore of the band gap of NCs to meet those of selected mediators and annihilators. The surface of colloidal NCs can be easily modified through ligand exchange or surface functionalization, which can enhance their stability and enable their integration into a variety of TTA-UC systems. Moreover, further doping and shell growth can be readily accomplished through colloidal synthesis to enhance the overall performance.

To the best of our knowledge, there have not been any reports on NCs prepared via physical vacuum methods used for TTA-UC applications. The main reason is the surface passivation and functionalization of NCs prepared via these methods is more difficult compared to colloidal NCs and limits the ability to optimize the surface chemistry, which affect the energy transfer and exciton dynamics in TTA-UC. However, as the field of TTA-UC continues to develop and new materials and synthesis methods are explored, it is possible that physically prepared NCs may be considered in future studies and applications.

3.2 | The size of NCs

The size of the NCs is a critical parameter that affects the TTA-UC efficiency, as the size directly correlates to the bandgap. In general, smaller NCs, with a larger surface area per unit volume, can provide larger driving force and electronic coupling, thus can enhance the efficiency of energy transfer between the NCs and the mediator molecules. However, if the size of the NCs is too small, they may suffer from significant surface defects and charge trapping, which can reduce their TTA-UC efficiency. Meanwhile, for a given annihilator it also narrows the apparent anti-Stokes shift of TTA-UC. The NCs size effect in triplet sensitization and TTA-UC has been reported for CdS NCs,^[76] CdSe NCs,^[82,95] PbS(Se) NCs^[108,111] and CsPbBr₃ perovskite NCs,^[140] as shown in Figure 4.

We recently investigated different-sized CdS NCs for visible-to-UV TTA-UC.^[76] The average diameters of these CdS NCs were 3.1 nm, 3.5 nm, and 4.3 nm. We observed that the medium sized CdS NCs exhibited the highest UCQY

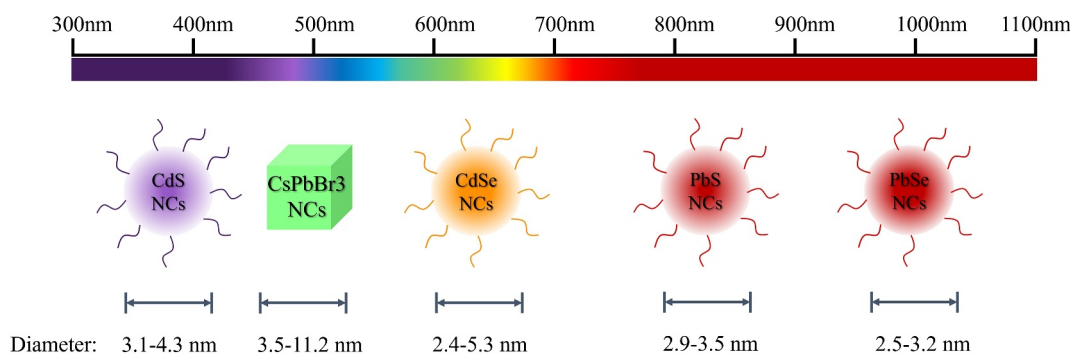


FIGURE 4 The size and absorption range of commonly used nanocrystals (NCs) in triplet-triplet annihilation photon upconversion (TTA-UC) systems.

($\Phi_{UC} = 10.4\%$) when matched with phenanthrene-3-carboxylic acid (3-PCA) as the mediator and 2,5-diphenyloxazole (PPO) as the annihilator, while the smaller-sized CdS NCs, with weaker absorbance in the visible range, resulted in a slightly reduced Φ_{UC} to 8.8%. The largest CdS NCs provided a smaller driving force for the energy transfer process, yielding Φ_{UC} of 6.0%.

Huang and co-workers studied size-dependence of CdSe NCs for visible range TTA-UC.^[95,140] They have found that as the CdSe NC diameter increases from 2.7 to 5.1 nm, Φ_{UC} decreases from 3.9% to less than 0.2%.^[140] The reduction in Φ_{UC} in this case is not only due to the decrease in the rate of TET from CdSe to the surface bound anthracene mediator, but also depends on the quality of CdSe NCs, which will be further discussed in the following section of NCs quality. By improving the quality of CdSe NCs, they have further investigated the TTA-UC performance of CdSe NCs with the diameter varied from 2.4 to 5.3 nm,^[95] and it was shown that 2.5 nm CdSe NCs had the highest Φ_{UC} of 7.9%. The efficiency of upconversion decreases with the size of CdSe NCs, except the smallest CdSe NCs (2.4 nm) with a Φ_{UC} of 6.4%.

A similar size dependence trend is also observed in PbS and PbSe NCs within the NIR-to-visible light range. The first solid-state NC-based TTA-UC thin films was reported using three sizes of PbS NCs with absorption peaks at 850 nm, 960 nm, and 1010 nm, respectively.^[108] The corresponding UCQY were found to be $(0.6 \pm 0.1)\%$, $(0.25 \pm 0.03)\%$, and $(0.11 \pm 0.02)\%$ for the three sizes of PbS NCs, respectively. Additionally, Mahboub et al. investigated solution-phase NIR-to-visible TTA-UC based on PbS (and PbSe) NCs.^[111] They observed a significant enhancement in upconverted light intensity by reducing the size of both PbS and PbSe NCs, achieving a 700-fold enhancement for PbS NCs from 3.5 to 2.9 nm and a 250-fold enhancement for PbSe NCs from 3.2 to 2.5 nm. However, the maximum UCQY in this study was only about 0.005%. Further improvement in the quality of NCs^[116] and introducing mediators^[109] has proven to be efficient ways to enhance NC-base NIR-to-visible TTA-UC.

Luo and co-workers investigated the size-dependent TET from perovskite NCs to surface attached 1-pyrene-carboxylic acid (PCA).^[140] They prepared cube-shaped

CsPbBr₃ NCs with varying edge lengths ranging from 3.5 to 11.2 nm. It was discovered that when the edge length exceeded 9.4 nm, the TET from CsPbBr₃ NCs to surface anchored PCA was hardly observed. In the case of CsPbBr₃ NCs, the influence of the driving force and spectral overlap was found to be negligible on the TET rate. Instead, the TET rate showed a linear scaling with the size-dependent carrier probability density at the NC surface, which is consistent with the Dexter-type TET mechanism that requires donor-acceptor wave function overlap.^[157-159]

3.3 | The length of surfactant ligands

The choice of surfactant ligands is another key factor for the colloidal stability and function of NCs.^[160-161] The formation of a surfactant layer around the NCs enables the dispersion of NC in the solution and can passivate surface defects by minimizing trap states. In general, longer carbon chain of the surfactant ligands would result in the synthesis of smaller particles with a narrower size distribution because of the slower diffusion of stearic acid. Increasing the length of the surfactant ligands would also enhance luminescence and quantum efficiency. When utilizing NCs in TTA-UC, achieving wave function overlap between NCs and energy acceptors is crucial. The magnitude of this coupling is expected to exhibit an exponential decay with distance. Therefore, the length of the surfactant chain plays a critical role in TTA-UC, as it involves a tradeoff between enhancing NCs quality and optimizing the efficiency of energy transfer. Finding the right balance is crucial to maximize the performance of NC-based TTA-UC systems.

In 2017, Nienhaus and co-workers investigated the triplet exciton transfer to rubrene from PbS NCs with different lengths of surfactant ligand in the solid-state.^[113] Eight different length of carboxylic acid ligands ranging from 4 to 18 carbon atoms resulted in the thickness of ligand shell changing from 6 to 13 Å, as shown in Figure 5a. The rate of TET from PbS NCs to rubrene is an order of magnitude enhanced when the aliphatic ligand length reduces from 18 to 4C, with saturation for ligand shell thicknesses ≤ 10 Å. The value of solid-state Φ_{UC} increased from $0.6 \pm 0.1\%$ for

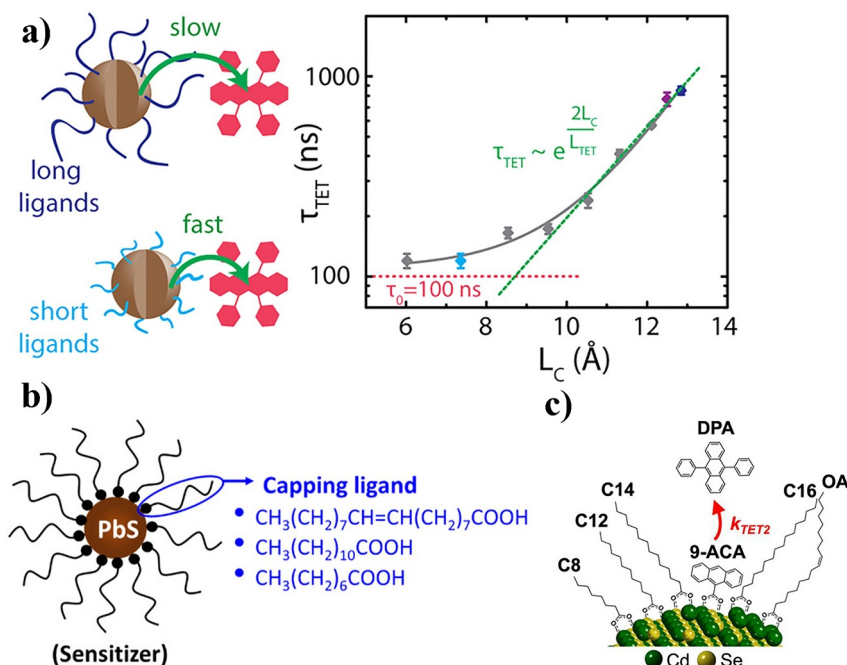


FIGURE 5 Nanocrystals (NCs) with varied length of surfactant ligands. (a) PbS NCs with carboxylic acid ligands ranging from 6 to 13 Å in length, and the TET time (τ_{TET}) to rubrene was exponentially increased with the ligand shell thicknesses (L_c). Reproduced with permission.^[113] Copyright 2017 American Chemical Society. (b) PbS NCs with three different lengths of carboxylic acid ligands with 8, 12 and 18 carbon atoms. Reproduced with permission.^[123] Copyright 2021 American Chemical Society. (c) CdSe NCs with four different carbon ligands to facilitate triplet exciton transfer to DPA. Reproduced with permission.^[106] Copyright 2022 American Chemical Society. DPA, 9,10-diphenylanthracene.

long oleic acid ligands to $3.5 \pm 0.5\%$ for shorter hexanoic acid ligands (C6).^[108] The authors noted that the shortest ligands (C4), which hinder long-term colloidal stability, offered little advantage for energy transfer. In 2021, Tripathi and co-workers studied the solution phase NIR-to-visible TTA-UC by directly attaching the emitter of 5,11-bis (triethylsilylethynyl)anthradithiophene (TES-ADT) to PbS NCs with three different lengths of carboxylic acid ligands (C8, C12 and C18).^[123] The rate and efficiency of TET from PbS to TES-ADT was enhanced with the short ligand. However, the PLQY of PbS NCs was decreased by introducing shorter ligands due to an increase in number of defect states. Competition between the acceleration of TET and non-radiative deactivation of the excited state led to an optimization of UCQY at the middle-length ligand (C12). In 2022, Miyashita and co-workers investigated surfactant ligands of CdSe NCs with four different lengths ranging from C8 to C16.^[106] A direct TET from CdSe NCs to the annihilator of DPA was observed when the surface ligand had a length of C8, which can eliminate the requirement for a mediator as TET relay. This resulted in a higher UCQY of 3.5% in the DPA and CdSe NCs system, compared to $<0.01\%$ when using ligands with 18 carbons.

3.4 | The shape of NCs

The shape of NCs also impacts the energy transfer from NCs to surface attached molecules. The shape-induced

modification of band structure, exciton relaxation and adsorbing molecules can be attributed to change in the radiative and non-radiative rates, and thus influence the energy transfer efficiency.^[162] Most published NC-based TTA-UC systems utilize spherical NCs due to the straightforward control of colloidal synthesis. On the one hand, the symmetrical shape allows for a uniform distribution of states and provides a high surface-to-volume ratio, enabling efficient surface functionalization and energy transfer. On the other hand, the non-spherical NCs can introduce preferential orientations and directional pathways for energy transfer processes. VanOrman and co-workers studied anisotropic CdSe nanoplatelets (NPLs) for green-to-blue upconversion^[101] and CdTe nanorods (NRs) for red-to-blue upconversion.^[102] CdSe NPLs exhibited a lower UC threshold than comparable CdSe spherical NCs, however, the UCQY of 2.7% in CdSe NPLs is lower than that of spherical NC-based TTA-UC systems. A low UCQY was attributed to the strong back-transfer caused by the large oscillator strength of the NPLs. Stacking of the NPLs also resulted in TET-inactive transmitter ligands or steric hindrance for accessing surface ligands for TTA-UC. A considerably lower UC threshold was observed in CdTe NRs, with $I_{th} = 93$ mW/cm². Authors suspected that the lower UCQY of 2.2% was possibly caused by internal grain boundaries of the NRs acting as undesired recombination centers. Moreover, the aggregation of the NRs can also introduce potential loss pathway analogous to NPLs stacking.

3.5 | The quality of NCs

Defects in NCs can have a negative impact on the efficiency of TTA-UC. Defects such as surface traps and non-radiative recombination centers can reduce the available energy for the process and interfering with the efficiency of TET at the interface. Therefore, it is important to minimize defects by improving the quality of the NCs. This can be achieved by carefully selecting precursor sources, the feed molar ratio, the reaction temperature and time, and the purification steps.^[163-164] Huang and co-workers reported the enhancement in NIR-to-yellow TTA-UC by synthetically improving the quality of the PbS NC.^[116] By using highly purified lead and thiourea precursors, the PLQY of PbS NCs can be as high as 34% and the corresponsive UCQY is 5.9%. For comparison, PbS NCs synthesized by using commercially available lead and sulfide precursors yielded a slightly lower PLQY of 30% and UCQY of 2.3%. The enhanced TTA-UC performance can be attributed to the longer intrinsic exciton lifetimes of high quality PbS NCs and the ability to support a longer triplet lifetime for the surface-bound mediators. In our recent study of visible-to-UV TTA-UC, the CdS NCs were synthesized at lower reaction temperature (less than 200 °C) with a longer annealing time (~1 h) and purified with modified hexane-acetonitrile precipitation.^[76] Compared to previously reported CdS NCs used for visible-to-UV TTA-UC,^[73] the PLQY of these CdS NCs was about 5-fold enhanced, which led to a significantly improved UCQY of 9.1%.^[76]

3.6 | Core-shell NCs

The synthesis of a shell on NCs has proven to be an efficient approach to improve the stability, remove surface traps, control surface chemistry, and tailor optical properties for various applications, including TTA-UC. It should be noted that the shell materials should preferably crystallize in the same structure as the core materials and exhibit a small lattice mismatch.^[165] The shell material and its interface engineering with the core and mediator also needs to be considered for optimizing energy transfer. Regarding the TTA-UC application, the shell works as a barrier between the NC core and the mediators/annihilator. Since the short-range Dexter-type processes from NCs is very sensitive to the distance, the thickness of the shell is a critical factor that influences the energy transfer efficiency.

CdS/ZnS and ZnSe/ZnS core/shell NCs have been reported in visible-to-UV TTA-UC systems, as shown in Figure 6a.^[73,79] The growth of ZnS shell on CdS NCs can passivate the surface traps to improve PLQY from 4.4% to 26% and increase the efficiency of TET to 90%. However, the ZnS shell also acts as a tunneling barrier for TET, which results in an optimal 4 monolayers of ZnS shell that maximizes the visible-to-UV UCQY of 2.6%.^[73] In the case of heavy metal-free ZnSe/ZnS core/shell NCs, a thermodynamic (slow) shelling method was used to minimize the formation of traps at the core/shell interface.^[166] To balance between defect passivation and TET efficiency, here a 1.4 monolayer ZnS

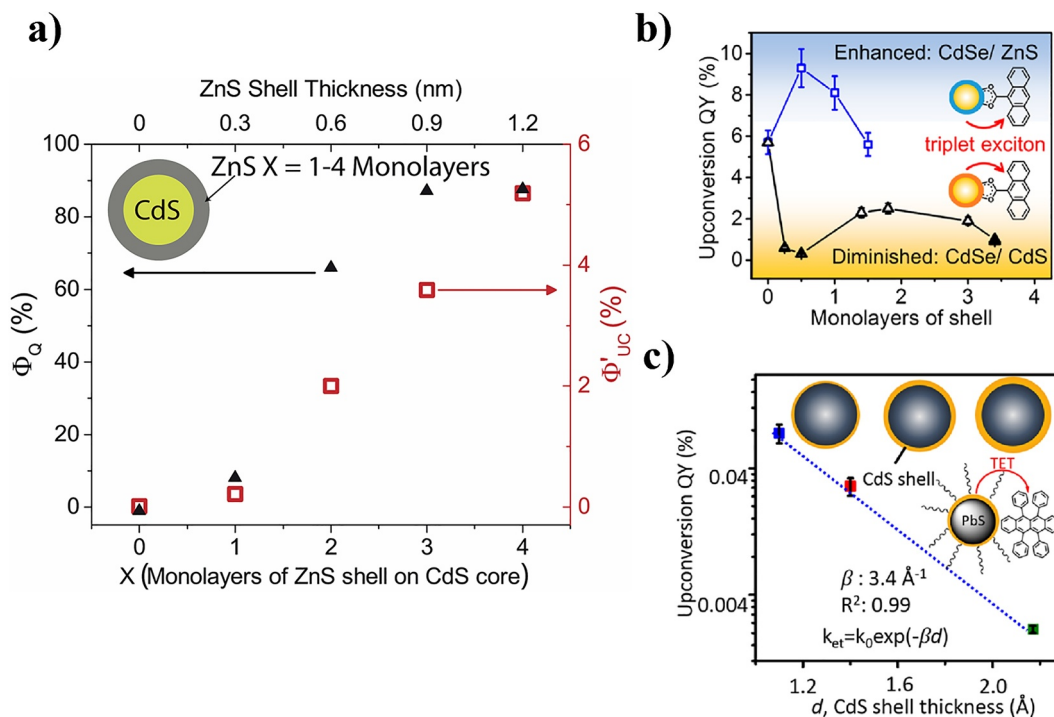


FIGURE 6 Core-shell nanostructures (NCs) used in triplet-triplet annihilation photon upconversion (TTA-UC) (a) photoluminescence (PL) quenching efficiency and upconversion quantum yield (UCQY) as a function of ZnS shell thickness on CdS NCs. Reproduced with permission.^[73] Copyright 2017, the Royal Society of Chemistry. (b) UCQY as a function of ZnS and CdS shell thickness on CdSe NCs. Reproduced with permission.^[88] Copyright 2018, American Chemical Society. (c) UCQY as a function of CdS shell thickness on PbS NCs. Reproduced with permission.^[110] Copyright 2016, John Wiley and Sons.

shell was grown on ZnSe NCs, leading a high PLQY of 78% and TET efficiency of ~73% that eventually resulted in UCQY of 3.1% in visible-to-UV light region.^[79]

The most common core/shell NCs for visible light range TTA-UC is CdSe/ZnS NCs.^[83,88,96] The first report was based on commercial CdSe/ZnS NCs without the detailed information on the shell thickness.^[83] Compared to commercial CdSe core-only NCs, the UCQY can be enhanced about 50-fold, although the overall UCQY was as low as 0.7%. The low UCQY in this case was possibly due to the non-optimized shell thickness and low TET efficiency to the mediator. Huang and co-workers further investigated the impact of shell thickness on the efficiency of TET and TTA-UC. CdS and ZnS shells with different shell thicknesses were grown on CdSe NCs (Figure 6 (b)). The shell enhanced TET by removing surface traps and increasing the exciton lifetime. It resulted in an optimal UCQY of ~4.6% for 1.5 monolayer of ZnS shell, and UCQY of 1.2% in 1.8 monolayer of CdS shell. The authors attributed the different effects of ZnS and CdS shell to the shorter exciton lifetime and increased exciton–phonon coupling of CdS.^[88] Wu's group reported non-toxic CuInS₂/ZnS and InP/ZnSe/ZnS core/shell NCs for visible range TTA-UC.^[90,94] A sub-monolayer of ZnS shell was grown onto the CuInS₂ NCs to improve their stability and dispersibility in the solution. Multi-shell structure of InP/ZnSe/ZnS NCs was introduced because the lattice constant of ZnSe lies between those of InP and ZnS.^[167] This multi-shell with a thickness of ~0.6 nm can passivate the trap states and provide long-term stability.

PbS/CdS core/shell NCs are generally used in NIR-to-visible TTA-UC, as shown in Figure 6c.^[110,114] A monolayer or sub-monolayer CdS shell on PbS NCs can enhance TET efficiency by passivating trap states to suppress competitive charge transfer and prolongs the lifetime of the mediator triplet excited state. The efficiency of TET and UCQY reduce with further growth of the shell because of the introduction of a large tunneling barrier. Very recently, non-toxic ZnCuInSe/ZnS core/shell NCs for NIR-to-visible TTA-UC was reported,^[124] and the 0.6 nm ZnS shell improved the stability of the NCs and prevented leakage of elements from the core. The high UCQY of 8.4% enabled the use of NIR light for organic synthesis and polymerization, which is further discussed in the application section.

In this section, we have provided a comprehensive summary of the key factors influencing the performance of TTA-UC using NCs. Although we have individually discussed the size, surfactant ligand, shape, quality, and shell of NCs, it is important to acknowledge that these factors collectively contribute to the overall performance. Thus, careful design and control of the NCs is paramount for achieving high performing TTA-UC systems. This involves meticulous attention to details, ensuring optimal size, appropriate surfactant ligands, desired shape, high-quality materials, and well-designed shells to enhance stability and balance between passivating trap state and efficient TET. Additionally, it is crucial to note that the exact mechanism of relaxation may vary between different systems, depending

on factors such as property of intrinsic materials, the surface quality, and anchoring groups. Understanding these nuances is vital for gaining insights into the relaxation process and further advancing the development of high-performing TTA-UC systems.

4 | MEDIATORS

Excited state lifetimes of the NCs are typically on the timescale of tens of nanosecond to a few microseconds, which is insufficient for diffusion-limited TET, therefore, mediators are frequently introduced by anchoring them onto the surfaces of the NCs through functional groups. These mediators play a crucial role in accepting triplet energy from the NCs and facilitating its transfer to the annihilators. In this section, we will focus on discussing how the anchoring group, number of anchored mediators, bridge length, and orientation of the mediators impact the performance of TTA-UC. However, it is worth noting that there are NC-based TTA-UC systems that are functionalized without introducing mediators. These systems rely on the direct energy transfer to annihilators through a Dexter-type process upon excitation across the band gap of NCs, and we will start with these designs first.

4.1 | NC-based TTA-UC without mediators

Two types of designs exist for NC-based TTA-UC without mediators. The first type relies on diffusion-controlled energy transfer between NCs and annihilators. This approach is generally feasible with PbS or PbSe NCs,^[81,108,111,113] which have longer PL lifetimes in the microsecond range and larger Bohr radii (the separation distance between electron and hole, 55 nm for PbSe, 21 nm for PbS), compared to CdSe (4 nm) and CdS (2 nm) NCs.^[168] Therefore, NIR-to-visible TTA-UC can be achieved by introducing for example, rubrene as the annihilator without the need for mediators. However, the overall UCQY is typically lower than 1%, and it only increases to 3.5% when a shorter hexanoic acid is utilized as the surfactant ligand for PbS NCs.^[113] The second type involves functionalizing the annihilators themselves with anchoring groups. For instance, by combining CdS/ZnS NCs with PPO as the annihilator, visible-to-UV TTA-UC can be achieved without a typical mediator.^[73] This could be attributed to the oxazole nitrogen of PPO binding to the ZnS surface, enabling short-distance Dexter-type energy transfer. Another example is TES-ADT, which was used as an annihilator for PbS NC-based TTA-UC.^[118,123] The thiophene group in TES-ADT allows close association with the PbS surface, which eliminates the need for additional mediators.

NC-based TTA-UC without mediators offers advantages such as simplified system design and the potential for a large apparent anti-Stokes shift. However, achieving efficient TTA-UC without mediators poses challenges. It necessitates

careful selection and design of the NCs and the annihilators to ensure efficient energy transfer.

4.2 | Approaches to introduce mediators

Before detailed discussion how the mediator impacts the efficiency of NC-based TTA-UC, we briefly explore the methods employed for anchoring the mediator to the surface of NCs. A common approach involves the ligand-exchange method, wherein the original ligands of the NCs are displaced by the mediator. This is generally carried out by mixing the mediators with the NCs solution and heating to an appropriate temperature, sometimes followed by sonication. After the ligand exchange reaction, the NCs anchored with mediators are separated from the excess ligands. This separation is typically accomplished through centrifugation or filtration, followed by multiple washes with a suitable solvent to eliminate any unreacted ligands or impurities.

In addition to the ligand-exchange method, our group and others also employ a direct mixing approach to introduce the mediator.^[76,91,101-102] This alternative method becomes particularly valuable when challenges arise with the ligand-exchange process, preventing a sufficient number of mediators loaded on the NCs' surface for efficient TTA-UC. The direct mixing approach facilitates efficient TET from the NCs, benefiting from the presence of both surface-bound ligands and dynamically weakly bound ligands. However, it is crucial to carefully select the concentration of the mediator when employing this approach to avoid potentially detrimental hetero-TTA between the annihilator and mediator, as well as reabsorption of upconverted photons.

4.3 | Anchoring groups

To relay the energy transfer between NCs and annihilator, the mediators are required to attach to the NCs surface via anchoring groups. The selection of suitable anchoring groups is crucial as they can impact the stability, solubility, surface chemistry, optical and electronic properties of NCs, as well as the properties of the interfaces and the energy transfer process. Previous studies have employed several common anchoring groups for the surface functionalization of NCs, including the carboxylic acid group,^[56,91-92,97-98,109,169-170] diphosphoric acid group,^[97] pyridyl moiety,^[83,85,100] and thiol ligands,^[87,123] as shown in Figure 7.

The carboxylic acid group as the most common anchoring group has been widely utilized to functionalize anthracene with CdSe NCs, tetracene with PbS or PbSe NCs, naphthalene or phenanthrene with perovskite NCs and CdS NCs.^[72,97,109,170] These carboxylic acid groups offer stability and chemical versatility. However, the carboxyl groups tend to be weakly bound to the surface of NCs, which can lead to surface saturation and detachment, limiting the density of attached functional groups and reducing the efficiency of the subsequent energy transfer process. The diphosphoric acid

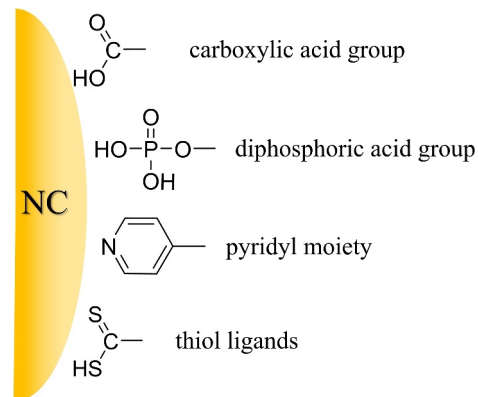


FIGURE 7 Commonly used anchoring groups for attaching mediators to nanocrystals (NCs).

group is an alternative functional group that binds to the surface of NCs through coordination bonds formed by the two phosphorus oxygens of the ligand.^[97] These bonds provide robust attachment and reduce the likelihood of detachment or surface saturation. However, it is associated with synthetic complexity of the desired mediators. The use of the diphosphoric acid group as an anchoring group may also lead to a reduction in the optoelectronic properties of NCs and restrict their solubility. The thiol ligands, typical heterocyclic anchoring group, can form coordination bonds with metal ions on the NCs' surface to achieve effective anchoring.^[87] This group exhibits robust coordination bonds, but they might induce delocalization of excitonic hole onto the ligands and inhibit TET across the interface.^[171-172] The linking ability of the pyridyl moiety to the surface of NCs is relatively weak.^[83,85,100] as it is through the non-covalent Lewis acid-base interactions between the pyridyl moiety and metal ions of the NCs. It is important to note that the specific linking abilities may vary depending on experimental conditions and molecular structures.

4.4 | The number of anchored mediators

The number of mediators on the surface of the NCs also strongly affects the performance of NC-based TTA-UC. Lian and co-workers investigated the TET process by anchoring oligothiophene carboxylic acid (T6) to the surface of CdSe NCs via mixing approach for triplet energy sensitization.^[91] The efficiency of TET from CdSe NCs to T6 increased when the T6 concentration increased, with $\Phi_{TET_1} = 15.4 \pm 0.6\%$ at a concentration of 50 mM to $31.8 \pm 1.2\%$ at a concentration of 375 mM. The low efficiency of TET can be explained by the average number of adsorbed T6 per CdSe NC is only around 0.5 at the highest concentration. We also used a mixing approach to introduce mediators on the surface CdS NCs, and efficient TET was observed with $\Phi_{TET_1} > 90\%$.^[76] This is achieved because the number of bound ligands can be estimated to be about 20 per CdS NC in our case.

However, considering the overall TTA-UC performance, it is important to note that having a larger number of

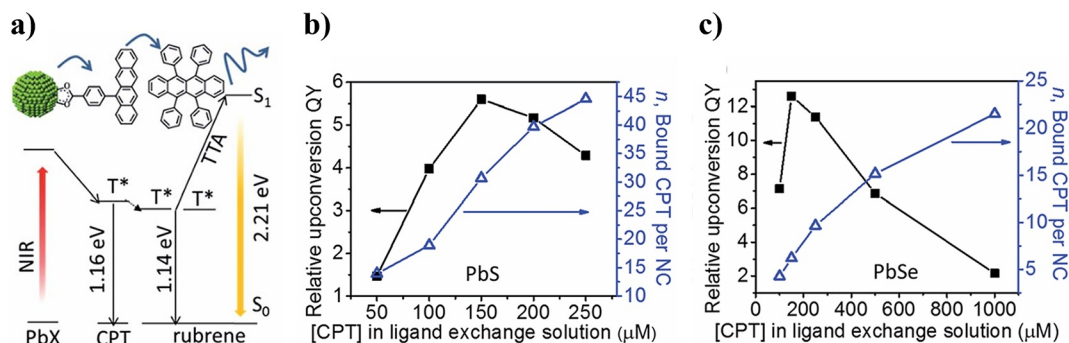


FIGURE 8 PbX (X = S, Se) nanocrystals (NCs) with varied number of surfactant ligands. (a) Schematic of PbX (X = S, Se) NC-based triplet-triplet annihilation photon upconversion (TTA-UC). (b) Relative upconversion quantum yield (UCQY) and bound number of the mediator to PbS NCs versus ligand concentration in the solution. (c) Relative UCQY and bound number of the mediator to PbSe NCs versus ligand concentration in the solution. Reproduced with permission.^[109] Copyright 2016, the Royal Society of Chemistry.

anchored mediators does not always guarantee higher upconversion efficiency. Huang et al. investigated mediator of 4-(tetracen-5-yl)benzoic acid (CPT) for the sensitized upconversion of NIR photons in PbS and PbSe NCs, as shown in Figure 8.^[109] The number of bound mediators varied from 14 to 45 per PbS NC (2.9 nm) and from 3 to 22 per PbSe NC (2.5 nm). The maximum UCQYs were achieved in the cases of 30 CPT molecules bound to one PbS NC and 5 CPT molecules bound to one PbSe NC. Further increasing the number of mediators on the surface causes a reduce in the UCQY, due to dye interactions between two nearby CPT molecules on the NC surface that suppresses the photon upconversion.

4.5 | Orientation

The positioning of the anchoring group on the mediator also takes an important role as it dictates the orientation of the attached mediator on the surface of the NCs. The orientation of the attached mediator on the surface of NCs impacts the electronic coupling (orbital overlap) between them. This, in turn, can affect the efficiency of energy transfer and ultimately influence the TTA-UC performance. Xia and co-workers studied anthracene with two functional groups, carboxylic acid and dithiocarbamate, that varied between the 1-, 2- and 9-positions, as shown in Figure 9. These anthracene isomers served as mediators for CdSe NCs and DPA for photon upconversion.^[87] In general, anthracene functionalized at the 1-position are more effective compared to the 2-position in mediating energy transfer. CdSe/9-ACA NCs showed the highest UCQY at around 6%, which was approximately 10 times higher than CdSe/2-ACA, while the CdSe/9-ADTC NCs had the lowest UCQY at 0.1%. Li and co-workers designed a series of bidentate bis(pyridine) anthracene isomers (2,3-PyAn, 3,3-PyAn, 2,2-PyAn) that differ in their binding geometries for CdSe NC-based TTA-UC.^[85] When the mediator binds via the two pyridine N atoms, the anthracene long-axis was parallel to the NC surfaces. They observed that the 2,3-PyAn isomer yielded the

highest UCQY of ~6.5%, followed by 3,3-PyAn (~4.1%) and 2,2-PyAn (~1.3%). Okumura and co-workers used one pyridine moiety for perpendicular binding of anthracene to the CdSe/CdS core-shell NCs. In this case it resulted in an UCQY of 0.7%.^[83]

He et al. further studied anthracene with the carboxylic acid group at 2- and 9-position, for TTA-UC based on CsPbBr₃ and CdSe NCs.^[99] They found that, in the case of CsPbBr₃ NCs, 2-ACA had a higher UCQY than 9-ACA, which was exactly opposite to previous observation for CdSe NCs. They explained the opposite trends from quantum confinement of NCs, which can strongly affect the electronic coupling between NCs and surface-anchored mediator. CdSe NCs are more strongly quantum-confined than CsPbBr₃ NCs, and tend to have higher carrier wavefunction amplitudes on NC surfaces,^[159] which favor the through-space electronic coupling between NCs and surface-anchored mediators. Coupling with 9-ACA is more efficient than 2-ACA in the case of CdSe NCs, due to the center of the anthracene moiety of 9-ACA is closer to NCs than that of 2-ACA. For weakly confined CsPbBr₃ NCs, the chemical resonance effect in 2-ACA enabled by the co-planar configuration between the carboxylate and anthracene moieties, opens up a through-bond coupling between NCs and 2-ACA.

4.6 | Bridge distance

As the energy transfer from NCs to the mediator is through a Dexter-type energy transfer, the efficiency of energy transfer is very sensitive to the length of the bridge group between NCs and the mediator. Li and co-workers investigated the distance-dependent TET from CdSe NCs to anthracene, in which a rigid aromatic and flexible aliphatic spacers with different lengths were used as the linkers (Figure 10a).^[84] The rate constant of TET and UCQY in the presence of a rigid aromatic linker exhibited an exponential dependence on the length of the bridge. It decreased with an increase in the number of phenyl groups from 0 to 2. Surprisingly, different lengths of flexible aliphatic bridges have no effect

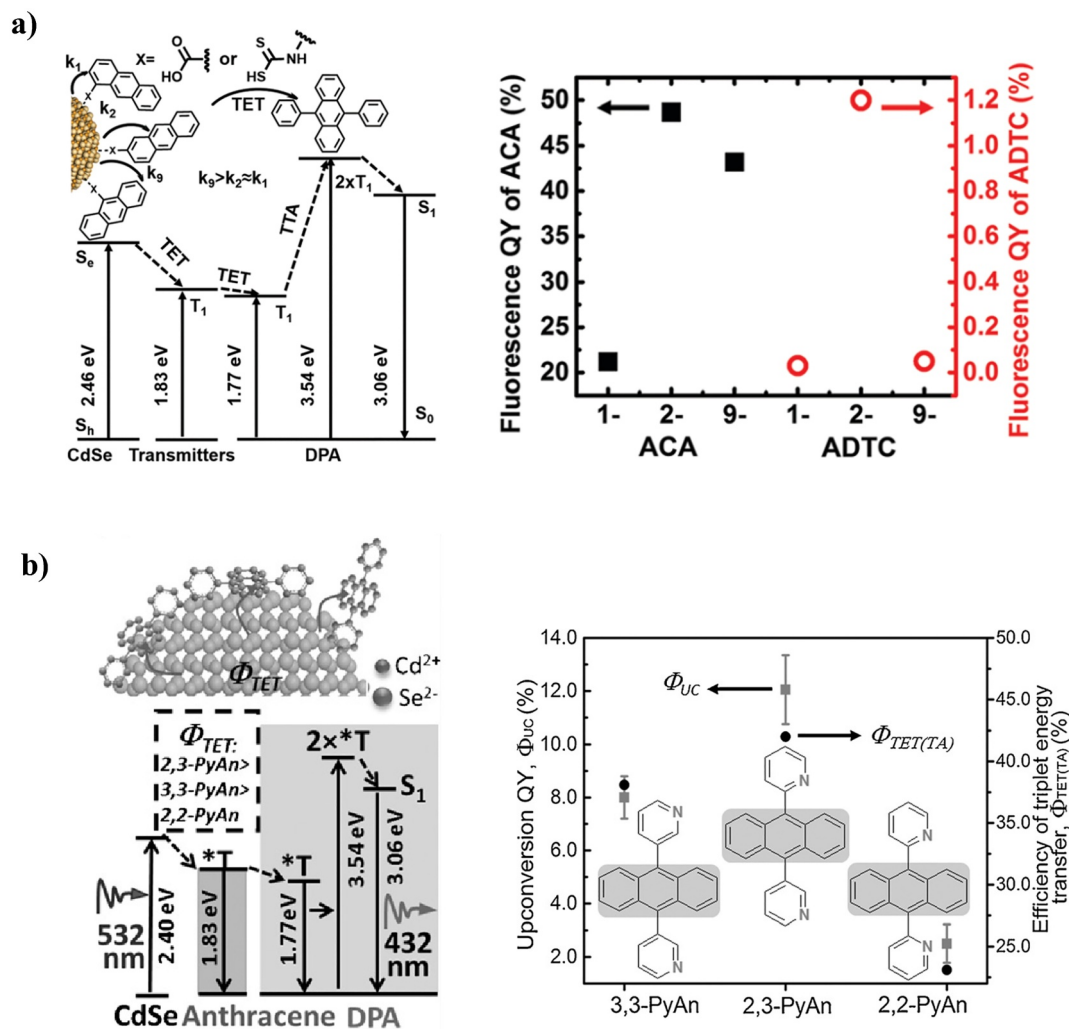


FIGURE 9 The effect of orientation of the mediator anchored on the surface of nanocrystals (NCs). (a) Schematic of the energy transfer with CdSe NCs as sensitizer and anthracene isomers as mediators (left), and the fluorescence quantum yields (QY) of anthracene isomers (right). Reproduced with permission.^[87] Copyright 2017, the Royal Society of Chemistry. (b) Schematic of the energy transfer with CdSe NCs as sensitizer and bis(pyridine) anthracene isomers as mediators (left), and the triplet energy transfer (TET) efficiency and the corresponding upconversion quantum yield (UCQY) for each bis(pyridine) anthracene isomers (right). Reproduced with permission.^[85] Copyright 2017, John Wiley and Sons.

on the rate of TET. Huang and co-workers further investigated the TET process from CdSe NCs to anthracene with the aromatic spacer linkers with a length of 0 to 5 phenylene unit, as shown in Figure 10b.^[100] They observed that the TET rate decreased exponentially when phenylene units were below 3. However, the TET rate increased again when the length of the rigid bridge was increased to 4 and 5 phenylene units. They explained that a transition from exciton tunneling to hopping resulted in relatively efficient and distance-independent TET beyond the traditional 1 nm Dexter distance.

Xu and co-workers designed PbS NC-based TTA-UC systems using the mediator molecules with the same tetracene triplet acceptor but varying length of phenyl linkers (Figure 10c).^[120] With increasing linker length, the efficiency of TET₁ from the PbS NC to the mediator decreased,

while the efficiency of TET₂ from the mediator to rubrene annihilators increased. The combined results led to a net decrease of UCQY with distance in the assemble of PbS NC-based TTA-UC systems.

To optimize the overall performance of NC-based TTA-UC systems from the mediators' perspective, various factors need to be taken into account. In addition to the energy alignment between NCs and the annihilator, considerations should include the choice of anchoring group, the number of anchored mediators on the NCs' surface, the orientation of the mediator, and the bridge distance between the NCs and the mediator. Achieving an optimal balance among these factors is crucial. By carefully adjusting and optimizing these parameters, it is possible to enhance the efficiency of energy transfer in NC-based TTA-UC systems, thus can lead to improve an overall performance.

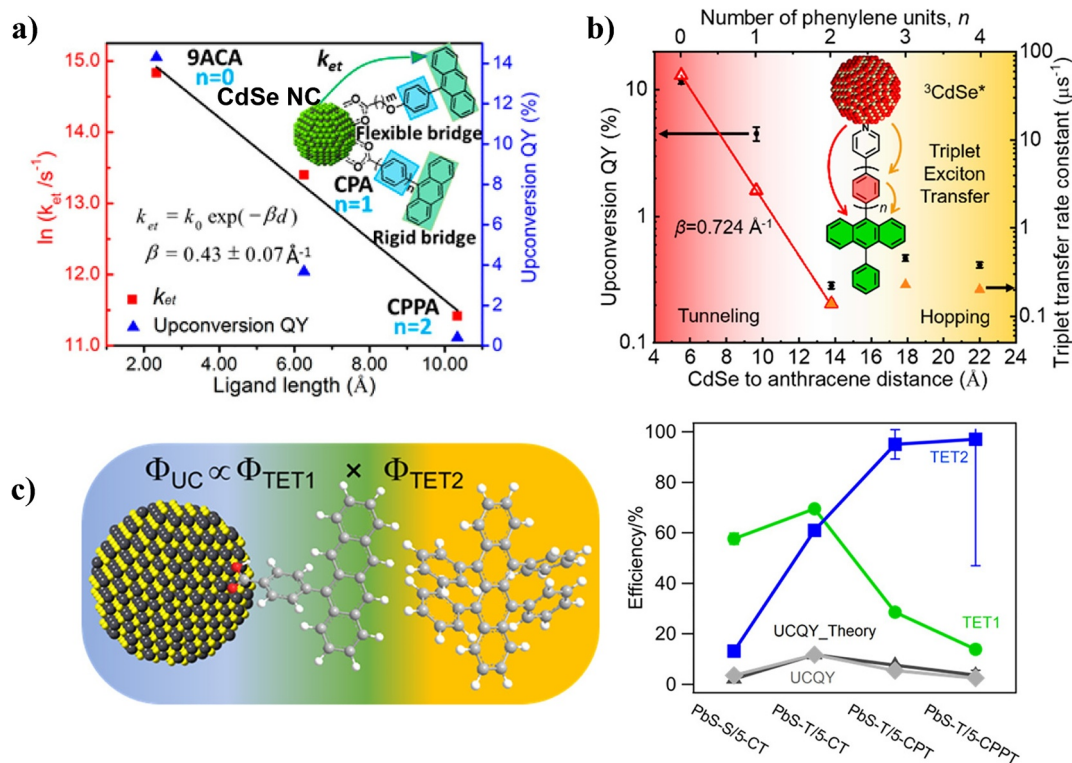


FIGURE 10 The bridge length dependence of NC-based triplet-triplet annihilation photon upconversion (TTA-UC). (a) upconversion quantum yield (UCQY) and triplet energy transfer (TET) rate as a function of bridge length in CdSe NC-bridge-anthracene hybrid system less than 10 Å and (b) longer than 10 Å. Reproduced with permission.^[84,100] Copyright 2016 and 2020, American Chemical Society. (c) Schematic of PbS nanocrystals (NCs) as sensitizer and tetracene mediators with $n = 0, 1,$ and 2 phenyl spacer groups (left), and efficiencies of TET_1 from the PbS NCs to the mediators (green circles), TET_2 from the mediator to rubrene annihilators (blue squares), calculated theoretical UCQY (black triangles), and measured UCQY (gray diamonds) of four indicated quantum dot (QD)/mediator combinations. Reproduced with permission.^[120] Copyright 2020, American Chemical Society.

5 | ANNIHILATORS

Compared to the sensitizers, less work has been devoted to the design of new annihilators. In order to achieve high UCQY, the requirements for the annihilators are: high PLQY (nearly 100%), long-lived triplet state (preferably on the millisecond time scale), and that the energy of the S_1 is lower than twice the energy of T_1 . It should be noted that twice the energy of T_1 cannot be too high to allow the access of other parasitic states, such as the first quintet state (E_{Q_1}) and the second excited triplet state (E_{T_2}).^[33] For photon upconversion sensitized by NCs, the most commonly used annihilators are quite limited and reported in Figure 3. For NC-based TTA-UC systems, PPO is generally used for visible-to-UV upconversion, DPA for green-to-blue upconversion, and rubrene for NIR-to-yellow upconversion. In 2019, Nishimura and co-workers showed that TES-ADT, with a triplet energy of 1.08 eV (1150 nm) and TTA efficiency of 20%, can upconvert to visible wavelengths with an excitation wavelength at 1100 nm. However, the PLQY of TES-ADT reduces significantly when the concentration increases, from 74% at 0.2 mM to 2.6% at 100 mM, mainly due to a conversion from S_1 to a pair of triplets (TT) through singlet fission at high concentration.^[173] Gholizadeh and co-workers used violanthrone-79 (V79) as the annihilator combined with

PbS NCs for upconversion of NIR light from below the silicon bandgap.^[121] They estimated that the T_1 state of V79 is between 0.94 and 0.98 eV, the PLQY is 25% in dilute solution, and the TTA efficiency is 0.65%.

6 | SOLID-STATE NC-BASED TTA-UC

As discussed earlier, many advancements have been made in the research on liquid-phase NC-based TTA-UC, in many cases resulting in UCQYs exceeding 10%. There is an urgent need for developing solid-state NC-based TTA-UC towards practical applications, especially in overcoming the Shockley-Queisser limit of photovoltaic cells. Baldo's research group conducted a series of research and structural optimization of solid-state devices, as indicated in Figure 11. In 2015, they developed a solid-state upconversion film by thermally evaporation of PbS NCs as sensitizers and rubrene as annihilators, and they achieved upconversion from $\lambda > 1000$ nm to the visible. However, this design exhibited a low UCQY about $0.6 \pm 0.1\%$ due to inadequate light absorption.^[108] Thereafter, they proposed an improved colloidal NC-sensitized solid-state upconversion device structure, by using an optical spacer layer and a silver film back reflector deposited by thermal evaporation.^[112] The optical spacer layers and a silver reflector

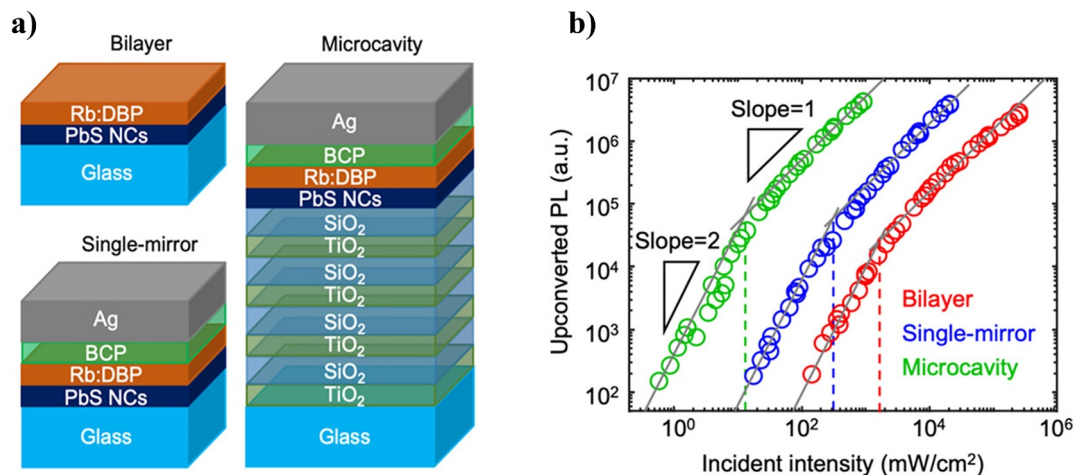


FIGURE 11 Interference-enhanced NIR-to-visible triplet-triplet annihilation photon upconversion (TTA-UC) in solid-state thin films. (a) Structure diagram of bilayer, single mirror, and microcavity devices. (b) Dependence of the upconverted (PL) on the incident intensity at $\lambda = 980$ nm. Reproduced with permission.^[122] Copyright 2021, the Authors.

optimized the interference effects to improve NIR light absorption. The output intensity of the upconverted emission at 610 nm was an order-of-magnitude enhanced by improving the infrared light absorption. Under the incident light intensity of 1.1 W/cm^2 , this device achieved an UCQY of $0.8 \pm 0.1\%$. In 2021, the same group further optimized the solid-state TTA-UC by integrating the upconversion layer into a Fabry-Perot microcavity.^[122] The structure of the microcavity consists of a distributed Bragg reflector (DBR) and a rear silver mirror with optical spacers. The DBR was composed of four pairs of quarter-wavelength-thick films of titanium dioxide and silicon dioxide, with a 90% reflectance at the pump wavelength of 980 nm. A layer of PbS NCs with the thickness of ~ 10 nm was spin-coated on the DBR. Then a 50 nm thick rubrene film doped with 1 vol% dibutyl phthalate, a bathocuproine (BCP) film as an optical spacer, and a 100 nm thick silver film were sequentially deposited by thermal evaporation. At the resonance wavelength of 980 nm, the absorption of the PbS NCs increased 74 times and the upconversion emission intensity increased 227 times. The threshold excitation intensity was reduced by 2 orders of magnitude to reach a subsolar flux of 13 mW/cm^2 .^[122] However, this design still exhibited a low UCQY of only $0.06 \pm 0.01\%$.

Shogo Amemori et al. prepared two hybrid materials that showed TTA-UC in the solid-state by combining NCs and metal-organic frameworks (MOFs, Figure 12).^[89] Green-to-blue TTA-UC was observed in the hybrid of an anthracene-based MOF and CdSe/CdS core-shell NCs, and NIR-to-yellow TTA-UC was observed in the hybrid of a tetracene-based MOF and PbS NCs. The UCQYs of this approach were very low (0.0009% at most), which could partly be due to low energy transfer efficiency from NCs to annihilator contained MOFs. Emily M. Rigsby et al. realized a TTA-UC film by drop casting the mixture of the polymer poly(9-vinylcarbazole), CdSe NCs functionalized with 9-ACA and DPA (Figure 13).^[104] The UCQY of the film reached 1.5% at a high excitation density exceeding 10 W/cm^2 .

The performance of NC-based TTA-UC in the solid state remains relatively low, especially in terms of UCQY. Therefore, further investigation is necessary to explore efficient approaches for fabricating solid-state TTA-UC systems. Taking experiences gained from molecular-sensitized TTA-UC could potentially help in achieving this goal. In 2007, Castellano and co-workers embedded a molecular sensitizer of PdOEP and DPA into a rubbery polymer matrix, and achieved the first example of incoherent low-power upconversion in a semi-solid polymer film.^[174] Subsequently, supramolecular, macromolecular, MOF structures, self-assembly, and hard-shell soft/liquid-core particles methods have emerged to overcome the diffusion limit of TTA-UC^[33,175] and the maximum UCQY in the solid state has been improved to approach 10%.^[176-179] These methods can be further applied in developing solid-state NC-based TTA-UC.

7 | APPLICATIONS OF NC-BASED TTA-UC SYSTEMS

Over the past decade, intensive efforts in developing NC-based TTA-UC have yielded significant improvements in upconversion efficiency and expansions of the wavelength range. This progress not only opens doors for further exploration of NC-based TTA-UC, but also makes it applicable towards practical applications such as solar energy harvesting and photochemical reactions using low-energy photons.^[180-181] Apart from the potential to enhance the efficiency of solar devices, NC-based TTA-UC enables enhanced light penetration because of the comparably long wavelength light used for excitation. Moreover, NC-based system offers easy redispersion and recycling of the materials, thanks to non-solvent surface ligands and ligand exchange capabilities of NCs. This feature provides flexibility, cost savings, and time efficiency in experimental

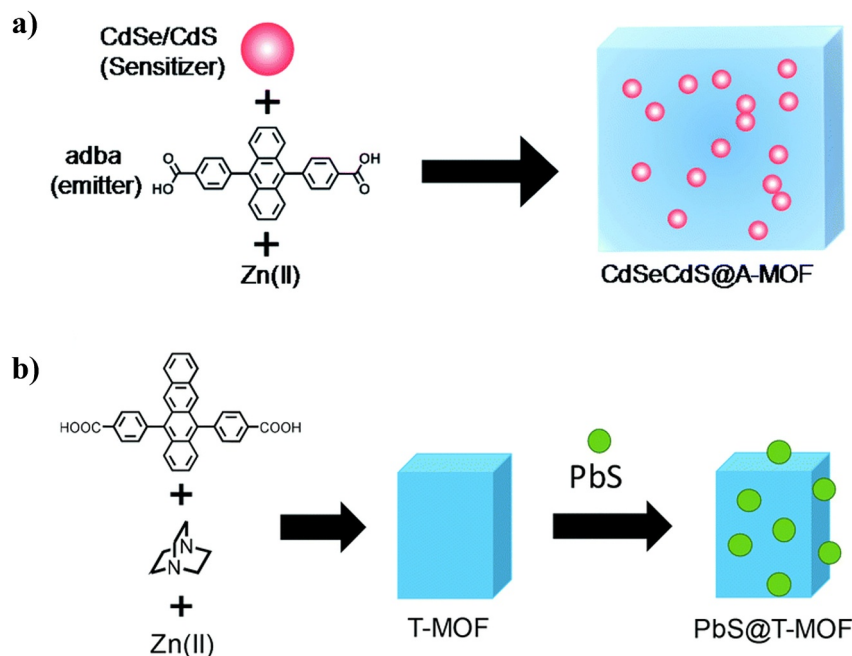


FIGURE 12 Solid-state approach by combining nanocrystals (NCs) and metal-organic frameworks (MOFs). (a) Schematic illustration of the CdSe/CdS@A-MOF for green-to-blue triplet-triplet annihilation photon upconversion (TTA-UC). (b) Schematic illustration of the PbS@T-MOF for NIR-to-visible TTA-UC. Reproduced with permission.^[89] Copyright 2018, the Royal Society of Chemistry.

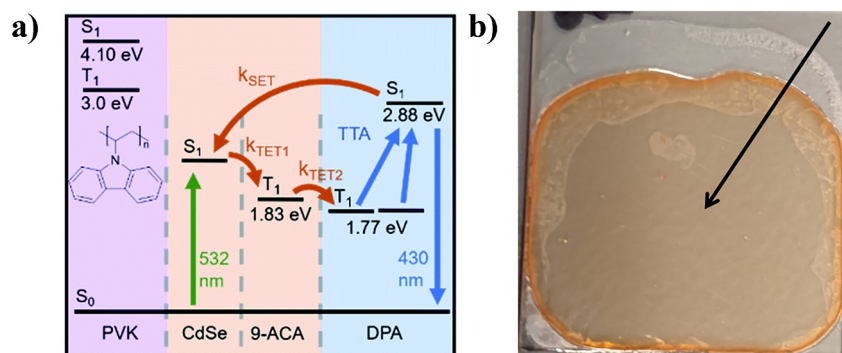


FIGURE 13 Solid-state approach by drop casting polymer and triplet-triplet annihilation photon upconversion (TTA-UC) components. (a) TTA-UC system of CdSe NCs-9-ACA-DPA combined PVK polymer. (b) The image of solid state TTA-UC in PVK thin film. Reproduced with permission.^[104] Copyright 2021, the Royal Society of Chemistry. PVK, polymer poly(9-vinylcarbazole).

applications. Although the broad absorption band of the NCs leads to the reabsorption of upconverted photons and subsequently decreases the external UCQY, it offers an advantage for practical applications. This advantage lies in its ability to maximize solar harvesting efficiency through both direct absorption and upconverted photon utilization.

7.1 | Solar energy harvesting

Combining TTA-UC sensitizer and annihilator pairs on metal oxide substrates is a common method to generate photocurrent by extracting charges directly from upconverted excited state.^[132,182] Shan and co-workers reported a family of photoelectrodes with upconverting NCs assemblies as the

photosensitizer. Bi-carboxylic acid derivatized anthracenes acts as both a bridge for anchoring CdSe NCs onto the oxide electrodes and an energy transfer acceptor for the excited state of CdSe, as shown in Figure 14a. Under green light illumination, the TTA-UC process resulted in the generation of high-energy singlet excitons, which enabled efficient electrons injection into the conduction band of n-type TiO₂ as the photoanode or hole injection into the valence band of p-type NiO as the photocathode. However, these upconverting assemblies still featured relatively low UCQY (<0.4%) at the surface of photoelectrodes. Further improving surface packing of the assemblies, replacing core/shell type NCs, and optimizing the chemical structure of annihilators could enhance the UCQY towards practical application in photoelectrocatalytic cells by using low-energy light for water splitting or CO₂ reduction.

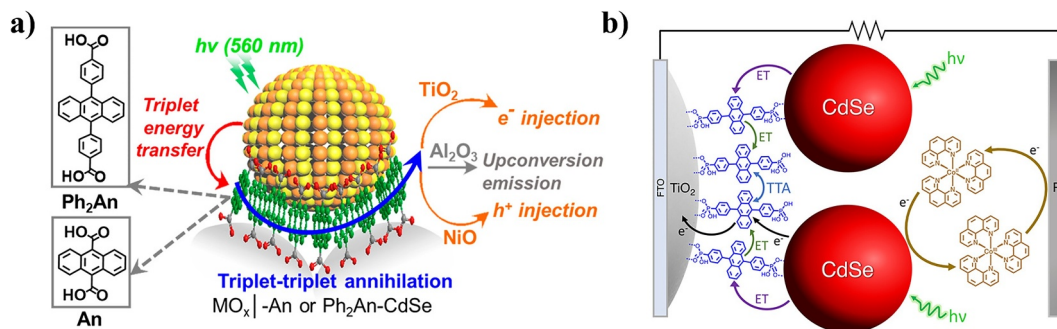


FIGURE 14 Generation of photocurrent by NC-based triplet-triplet annihilation photon upconversion (TTA-UC) system. (a) The assemblies of CdSe NC-based TTA-UC allowing to inject charge into the conduction band of TiO_2 at the photoanode and the valence band of NiO at the photocathode. Reproduced with permission.^[192] Copyright 2018, American Chemical Society. (b) Schematic illustration of integrated TTA-UC solar cell composed of nanocrystalline TiO_2 photoanodes and CdSe NC-based TTA-UC system. Reproduced with permission.^[130] Copyright 2019, American Chemical Society.

In 2019, Beery and co-workers integrated CdSe NCs as the sensitizer in an integrated TTA-UC solar cell. The photoanode consists of TiO_2 , phosphonated DPA acceptor molecules, and CdSe NCs sensitizers in a layered architecture, as shown in Figure 14b.^[130] Under AM1.5G solar irradiation, sensitization and TTA process allow to inject an electron to the conduction band of a fluorine-doped tin oxide electrode. The maximum efficiency onset threshold is reported to be 0.9 mW/cm^2 and the photocurrent gain of this design is $29 \mu\text{A/cm}^2$. The performance of this design is lower than those of the previous molecular sensitized device,^[183-185] due to lower sensitizer surface loadings, low energy transfer yield, slow regeneration kinetics, and competitive CdSe excited state quenching by redox processes. Further improving TTA-UC performance and optimizing of TTA-UC solar cell design will pave the way for practical application in enhancing solar energy harvesting.

7.2 | Photochemistry

NC-based photon upconversion allows further applications in photochemical reactions to be developed, such as photopolymerization and photo redox reactions, by taking advantages of the longer penetration distance of lower energy photons and broaden absorption bands of NCs. Imperiale and co-workers reported that a red-to-blue TTA-UC system based on ultra-small PbS NCs can facilitate the photo-initiated polymerization of methyl methacrylate (MMA) using long-wavelength light.^[105] The UC solution was mixed with monomeric MMA, a photoinitiator (methyl α -bromophenyl acetate) and a cross-linking additive (ethylene glycol dimethacrylate). The upconverted spin-singlet excited state of DPA enable to activate the homolytic cleavage of the initiator. Upon irradiation at 637 nm (40 mW) for 30 min, the formation of a poly (MMA) (PMMA) gel can be observed. The efficiency of photo-initiated polymerization is lower than direct blue light irradiation due to the low UCQY of this system.

Recently, Jiang and co-workers reported a NIR-to-yellow TTA-UC system employing PbS QDs to facilitate photoredox catalysis in the NIR II (NIR-II) region (1000–1700 nm). They

utilized a polymer matrix composed of MMA and ethylene glycol dimethacrylate in a 1:1 volume ratio, with ethyl α -bromophenylacetate (EBP) serving as the initiator. A summary table of the experimental conditions and outcomes is presented in Figure 15a. The experimental results demonstrated that complete polymerization was achieved upon 5 minutes laser irradiation at 1064 nm (152.9 W/cm^2).^[125] Degradation of the ultra-small PbS NCs was observed in the presence of an active radical catalyst after extended irradiation time. The overall efficiency of this photochemical reaction should be further optimized by developing photostable ultra-small NCs and improving the UCQY.

In the process of non-toxic development, Liang and co-workers reported a NIR-to-yellow upconversion system based on a non-toxic zinc-doped CuInSe_2 NCs with 5-CT as the mediator and rubrene as the annihilator, as shown in Figure 15b.^[124] The upconverted energy to singlet excited state of rubrene allows to perform NIR light induced reduction and oxidation. Three photoreactions mixed in the upconversion solution were tested upon illumination at 808 nm (400 mW, 1.3 W/cm^2): (a) dehalogenation of α -bromoacetophenone; (b) oxidation of an amine; (c) photoreduction of α -bromoacetophenone in the presence of phenol, see Figure 15c. After 8 h of 808 nm illumination, the yields of these photoreactions were 99%, 89%, and 97%, respectively. This TTA-UC system was further employed as the photo initiator for the free-radical polymerization of trimethylolpropane-triacrylate and the cationic polymerization of (3,4-epoxycyclohexane) methyl and 3,4-epoxycyclohexylcarboxylate (EPOX), see Figure 15c. The formation of a polymer gel was observed within 12 min of 808 nm illumination. It is worth noting that, although it is common that increasing the concentration of NCs can cause reduction of the UCQY because of the strong reabsorption, the efficiency of TTA-UC assisted photoreactions simply increases with the sensitizer concentration. This is due to that highly concentrated NCs cause reduction in the intensity threshold. The energy of the annihilator singlet excited states is involved in driving the photoreactions at short time scales before detrimental processes such as reabsorption, aggregation and quenching can occur. By taking advantage of the

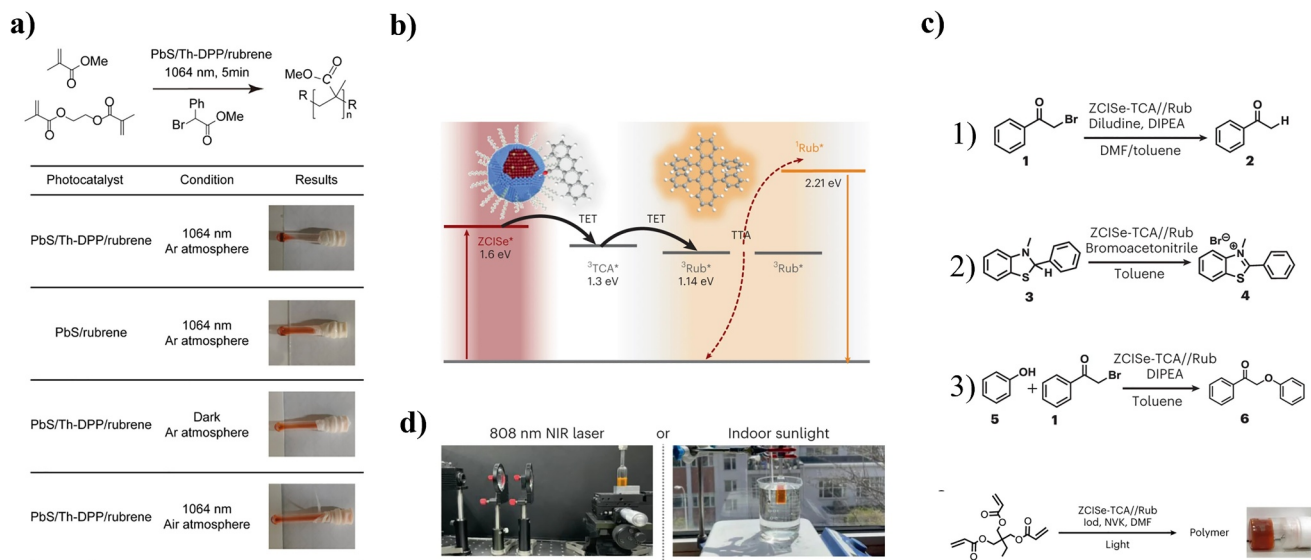


FIGURE 15 (a) Summary table of NIR-II driven photopolymerization using PbS quantum dot (QD)/Th-DPP/rubrene as a photocatalyst upon photoexcitation at 1064 nm. Reproduced with permission.^[125] Copyright 2024, American Chemical Society. (b) Schematic of near-infrared (NIR) light induced photoreactions of using zinc-doped CuInSe₂ (ZCISE) NC-based triplet-triplet annihilation photon upconversion (TTA-UC) system containing the ZCISE sensitizer, 5-tetracene carboxylic acid (5-CT) transmitter and rubrene annihilator. (c) Schematic of three photoreactions and the polymerization of trimethylolpropane-triacrylate (TMPTA). (d) Photograph of the reaction setup under 808 nm continuous-wave laser illumination (400 mW, left) or indoor solar illumination ($\sim 32 \text{ mW cm}^{-2}$, right). Reproduced with permission.^[124] Copyright 2024, Springer Nature Limited.

broad absorption band of NCs, TTA-UC assisted photoreactions show higher efficiency under the sunlight through indoor window ($\sim 32 \text{ mW cm}^{-2}$), Figure 15d. It took only 1 h to reach a 91% yield for dehalogenation of α -bromoacetophenone, 2 h for a 95% yield for the amine oxidation and 0.5 h for a 96% yield in for C-O bond formation. The acceleration of these photoreactions was achieved by capturing both visible and NIR photons that are abundant in sunlight through the photochemistry of triplet sensitization and upconversion.

8 | CONCLUSION AND PERSPECTIVES

NCs have proven to be highly attractive materials in the development of versatile TTA-UC systems, and the performance has been improved in this field over the past decade. The remarkable properties of NCs, including high energy transfer efficiency, small singlet-triplet energy splitting, broad and tunable spectral range, make them promising sensitizers towards TTA-UC application in solar energy harvesting and other applications. In this review, we have introduced the fundamental mechanism of NC-based TTA-UC and analyzed the key factors influencing upconverted performance from a materials perspective. Since the investigation of NC-based TTA-UC systems is relatively recent, there is limited research on solid-state approaches and applications, but these studies have demonstrated the immense potential of NC-based TTA-UC and have provided valuable insights for future investigations.

Compared to molecular sensitizers-based TTA-UC, which have achieved the highest UCQY approaching

42%,^[136] there is still considerable room for improving the performance of NC-based TTA-UC. This can be accomplished through several approaches, including: (a) utilizing high-quality NCs with minimal trap-state defects; (b) improving the efficiency of TET from NCs to the mediator or directly to the annihilator; (c) exploring alternative annihilators that can offer new possibilities.

By using NCs, TTA-UC system has achieved upconversion beyond the band gap of crystalline silicon,^[118,121] with the longest wavelength for excitation at 1100 nm, which is very challenging for molecularly sensitized TTA-UC. This is still far from covering the vast NIR light region, that is, from 750 to 2500 nm. In principle, NCs could do this as there are many potential NC candidates that can be utilized, such as PbTe NCs, Ag₂Se NCs. Further investigations should focus on the development and optimization of tailored annihilators to bridge the wavelength gap and enable efficient upconversion of NIR light, thereby broadening the scope of NC-based TTA-UC systems.

There are also several challenges that need to be addressed for NC-based TTA-UC. In the organic sensitizer-based systems, the accurate triplet energy level of organic molecules can be determined by theoretical calculation and low-temperature measurements. It has been reported that an endothermic energy transfer can occur when the T_1 of the organic sensitizer is lower than that of the annihilator. However, this endothermic energy transfer has not been observed in NC-based system, which possibly due to the inherent size distribution of the NCs that leads to the inaccurate estimation in T_1 energy levels. Microfluidic synthesis technology can be used to synthesize uniformly stable NCs materials with small size distribution. Another challenge is

that most NCs, such as traditional cadmium-based, lead-based and perovskite NCs, typically have strong absorption in the UV-visible region. For TTA-UC, high absorption in this region can cause a reabsorption of the upconverted photons, which leads to a reduction in the upconversion quantum efficiency of the TTA-UC system. Therefore, it is desired to design NCs materials with low absorption in the UV-visible region. Replacing the ligands of NCs with functional groups that minimize interaction with light in the UV-visible region or grow a well-controlled shell to confine the electronic states and reduce broad absorption tails can be further deeply investigated to meet this aim. However, considering practical applications in harvesting solar energy and solar cells, the 1-2 orders of magnitude larger molar absorption coefficient and the broader absorption region of NCs than organic materials can efficiently harvest light over a wide range of wavelengths and increases the probability of capturing incident photons. In addition to the requirements for solid-state approaches, which can be optimized by learning lessons from molecular sensitizers-based TTA-UC. These challenges include the development of scalable synthesis methods for NCs and enhancing the stability of the system under long-term irradiation. To enable large-scale production and implementation of NC-based TTA-UC systems, it is essential to develop synthesis methods that can reliably produce high-quality NCs with precise control over their size, composition, and surface properties. The materials and structures employed should be capable of withstanding extended exposure to light without significant degradation. Understanding the degradation mechanisms and developing strategies to enhance the stability of the system will be crucial for ensuring its long-term functionality and reliability.

Use of long-wavelength light will allow NC-based TTA-UC to further be used in bioimaging and biomedicine applications. It is essential to design water-soluble NCs and address potential toxicity concerns associated with Cd and Pb materials. Wu's research group have realized non-toxic InP/ZnSe/ZnS core-shell NCs and zinc-doped CuInSe₂ NCs for TTA-UC.^[94,124] Tang's group realized silicon NC-based TTA-UC and achieved air-stable fusion of triplet excitons in oil-in-water micelles.^[103] Exploring the synergies between TTA-UC research and biological application can pave the way for innovative technologies and advancements.

In conclusion, this review summarizes the progress of NC-based TTA-UC and emphasizes the need for further investigations to advance this field. Ongoing research is expected to drive the evolution of TTA-UC as a powerful tool for photon management and enable practical applications to sustainable energy solutions.

AUTHOR CONTRIBUTIONS

Kezhou Chen: Conceptualization; writing - original draft; investigation. **Qingxin Luan:** Conceptualization; writing - original draft; investigation. **Tiegen Liu:** Writing - review & editing; visualization; conceptualization; supervision. **Bo Albinsson:** Conceptualization; investigation; funding acquisition; project administration; writing - review & editing;

supervision. **Lili Hou:** Conceptualization; investigation; funding acquisition; writing - original draft; writing - review & editing; project administration; supervision.

ACKNOWLEDGEMENTS

L.H. acknowledges supports from National Key Research and Development Project of China (2023YFB3609300) and National Natural Science Foundation of China (62205240,12274320). L.H. and B.A. acknowledge support from Chalmers Genie program. B.A. acknowledges support from the Swedish research council (2022-03028).

CONFLICT OF INTEREST STATEMENT

The authors declare no conflict of interests.

DATA AVAILABILITY STATEMENT

The data that support the findings of this study are available on request from the corresponding author. The data are not publicly available due to privacy or ethical restrictions.

ORCID

Qingxin Luan  <https://orcid.org/0009-0000-9233-7126>

Lili Hou  <https://orcid.org/0000-0001-9453-4924>

REFERENCES

1. E. Kabir, P. Kumar, S. Kumar, A. A. Adelodun, K.-H. Kim, *Renewable Sustainable Energy Rev.* **2018**, *82*, 894.
2. S. Kalogirou, *Solar Energy Engineering: Processes and Systems*, Academic Press, Amsterdam **2014**.
3. N. S. Lewis, *Science* **2016**, *351*, 351.
4. B. Parida, S. Iniyar, R. Goic, *Renewable Sustainable Energy Rev.* **2011**, *15*, 1625.
5. P. Würfel, U. Würfel, *Physics of Solar Cells: From Basic Principles to Advanced Concepts*, 3rd ed., Wiley-VCH, Weinheim, Germany **2009**.
6. Y. Tian, C. Y. Zhao, *Appl. Energy* **2013**, *104*, 538.
7. P. Tao, G. Ni, C. Y. Song, W. Shang, J. B. Wu, J. Zhu, G. Chen, T. Deng, *Nat. Energy* **2018**, *3*, 1031.
8. D. A. Bainbridge, K. L. Haggard, R. Aljilani, *Passive Solar Architecture: Heating, Cooling, Ventilation, Daylighting, and More Using Natural Flows*, Chelsea Green Publishing, White River Junction, VT **2011**.
9. X. D. Sun, S. Y. Jiang, H. W. Huang, H. Li, B. H. Jia, T. Y. Ma, *Angew. Chem., Int. Ed.* **2022**, *61*, e202204880.
10. Q. Wang, M. Nakabayashi, T. Hisatomi, S. Sun, S. Akiyama, Z. Wang, Z. H. Pan, X. Xiao, T. Watanabe, T. Yamada, N. Shibata, T. Takata, K. Domen, *Nat. Mater.* **2019**, *18*, 827.
11. T. Hisatomi, K. Domen, *Nat. Catal.* **2019**, *2*, 387.
12. J. K. Stolarczyk, S. Bhattacharyya, L. Polavarapu, J. Feldmann, *ACS Catal.* **2018**, *8*, 3602.
13. J. G. Hou, S. Y. Cao, Y. Z. Wu, Z. M. Gao, F. Liang, Y. Q. Sun, Z. S. Lin, L. C. Sun, *Chem. Eur J.* **2017**, *23*, 9481.
14. J. Polo, M. Alonso-Abella, N. Martín-Chivelet, J. Alonso-Montesinos, G. López, A. Marzo, G. Nofuentes, N. Vela-Barrionuevo, *Energy* **2020**, *190*, 116453.
15. W. Shockley, H. J. Queisser, *J. Appl. Phys.* **1961**, *32*, 510.
16. S. Ruhle, *Sol. Energy* **2016**, *130*, 139.
17. B. S. Richards, D. Hudry, D. Busko, A. Turshatov, I. A. Howard, *Chem. Rev.* **2021**, *121*, 9165.
18. J. Zhou, Q. Liu, W. Feng, Y. Sun, F. Y. Li, *Chem. Rev.* **2015**, *115*, 395.
19. M. J. Y. Tayebjee, D. R. McCamey, T. W. Schmidt, *J. Phys. Chem. Lett.* **2015**, *6*, 2367.

20. D. Beery, T. W. Schmidt, K. Hanson, *ACS Appl. Mater. Interfaces* **2021**, *13*, 32601.
21. T. Trupke, M. A. Green, P. Würfel, *J. Appl. Phys.* **2002**, *92*, 4117.
22. A. Shalav, B. S. Richards, T. Trupke, R. P. Corkish, K. W. Kramer, H. U. Gudel, M. A. Green, in *3rd World Conference on Photovoltaic Energy Conversion*, Osaka, Japan **2003**, pp. 248–250.
23. R. W. Boyd, *Nonlinear Optics*, 4th ed., Academic Press, London **2020**.
24. Y. R. Shen, *The Principles of Nonlinear Optics*, Wiley, New York; Chichester **1984**.
25. G. Y. Chen, H. L. Qju, P. N. Prasad, X. Y. Chen, *Chem. Rev.* **2014**, *114*, 5161.
26. S. H. Wen, J. J. Zhou, K. Z. Zheng, A. Bednarkiewicz, X. G. Liu, D. Y. Jin, *Nat. Commun.* **2018**, *9*, 2415.
27. C. Simpson, T. M. Clarke, R. W. MacQueen, Y. Y. Cheng, A. J. Trevitt, A. J. Mozer, P. Wagner, T. W. Schmidt, A. Nattestad, *Phys. Chem. Chem. Phys.* **2015**, *17*, 24826.
28. T. F. Schulze, J. Czolk, Y.-Y. Cheng, B. Fückel, R. W. MacQueen, T. Khoury, M. J. Crossley, B. Stannowski, K. Lips, U. Lemmer, A. Colsmann, T. W. Schmidt, *J. Phys. Chem. C* **2012**, *116*, 22794.
29. T. Morifuji, Y. Takekuma, M. Nagata, *ACS Omega* **2019**, *4*, 11271.
30. Z. Huang, C.-H. Tung, L.-Z. Wu, *Acc. Mater. Res.* **2024**, *5*, 136.
31. O. S. Kwon, H. S. Song, J. Conde, H. I. Kim, N. Artzi, J. H. Kim, *ACS Nano* **2016**, *10*, 1512.
32. L. Huang, L. Zeng, Y. Z. Chen, N. Yu, L. Wang, K. Huang, Y. Zhao, G. Han, *Nat. Commun.* **2021**, *12*, 122.
33. V. Gray, K. Moth-Poulsen, B. Albinsson, M. Abrahamsson, *Coord. Chem. Rev.* **2018**, *362*, 54.
34. S. N. Sanders, T. H. Schloemer, M. K. Gangishetty, D. Anderson, M. Seitz, A. O. Gallegos, R. C. Stokes, D. N. Congreve, *Nature* **2022**, *604*, 474.
35. D. K. Limberg, J. H. Kang, R. C. Hayward, *J. Am. Chem. Soc.* **2022**, *144*, 5226.
36. S. Ji, W. Wu, W. Wu, H. Guo, J. Zhao, *Angew. Chem., Int. Ed.* **2011**, *50*, 1626.
37. R. S. Khnayzer, J. Blumhoff, J. A. Harrington, A. Haefele, F. Deng, F. N. Castellano, *Chem. Commun.* **2012**, *48*, 209.
38. Z. Jiang, M. Xu, F. Y. Li, Y. L. Yu, *J. Am. Chem. Soc.* **2013**, *135*, 16446.
39. S. Guo, W. Wu, J. Zhao, *Sci. Sin. Chim.* **2012**, *42*, 1381.
40. A. P. Alivisatos, A. L. Harris, N. J. Levinos, M. L. Steigerwald, L. E. Brus, *J. Chem. Phys.* **1988**, *89*, 4001.
41. L. Jacak, P. Hawrylak, A. Wójs, *Quantum Dots*, Springer, Berlin **2012**.
42. A. P. Alivisatos, *Science* **1996**, *271*, 933.
43. Y. S. Park, J. Roh, B. T. Diroll, R. D. Schaller, V. I. Klimov, *Nat. Rev. Mater.* **2021**, *6*, 382.
44. Y. Shirasaki, G. J. Supran, M. G. Bawendi, V. Bulovic, *Nat. Photonics* **2013**, *7*, 13.
45. Y. F. Shu, X. Lin, H. Y. Qin, Z. Hu, Y. Z. Jin, X. G. Peng, *Angew. Chem., Int. Ed.* **2020**, *59*, 22312.
46. D. V. Talapin, J. S. Lee, M. V. Kovalenko, E. V. Shevchenko, *Chem. Rev.* **2010**, *110*, 389.
47. M. X. Liu, N. Yazdani, M. Yarema, M. Jansen, V. Wood, E. H. Sargent, *Nat. Electron.* **2021**, *4*, 548.
48. G. H. Carey, A. L. Abdelhady, Z. J. Ning, S. M. Thon, O. M. Bakr, E. H. Sargent, *Chem. Rev.* **2015**, *115*, 12732.
49. A. J. Nozik, M. C. Beard, J. M. Luther, M. Law, R. J. Ellingson, J. C. Johnson, *Chem. Rev.* **2010**, *110*, 6873.
50. T. Jamieson, R. Bakhshi, D. Petrova, R. Pocock, M. Imani, A. M. Seifalian, *Biomaterials* **2007**, *28*, 4717.
51. W. C. W. Chan, D. J. Maxwell, X. H. Gao, R. E. Bailey, M. Y. Han, S. M. Nie, *Curr. Opin. Biotechnol.* **2002**, *13*, 40.
52. M. Liu, P. Xia, G. Zhao, C. Nie, K. Gao, S. He, L. Wang, K. Wu, *Angew. Chem., Int. Ed.* **2022**, *61*, e202208241.
53. L. Hou, W. Larsson, S. Hecht, J. Andréasson, B. Albinsson, *J. Mater. Chem. C* **2022**, *10*, 15833.
54. Y. Jiang, R. Lopez-Arteaga, E. A. Weiss, *J. Am. Chem. Soc.* **2022**, *144*, 3782.
55. Y. Lin, M. Avvacumova, R. Zhao, X. Chen, M. C. Beard, Y. Yan, *ACS Appl. Mater. Interfaces* **2022**, *14*, 25357.
56. C. Mongin, S. Garakyaraghi, N. Razgoniaeva, M. Zamkov, F. N. Castellano, *Science* **2016**, *351*, 369.
57. M. W. Brett, C. K. Gordon, J. Hardy, N. J. L. K. Davis, *ACS Phys. Chem. Au* **2022**, *2*, 364.
58. J. T. DuBose, P. V. Kamat, *ACS Energy Lett.* **2022**, *7*, 1994.
59. R. Weiss, Z. A. VanOrman, C. M. Sullivan, L. Nienhaus, *ACS Mater. Au* **2022**, *2*, 641.
60. N. A. Romero, D. A. Nicewicz, *Chem. Rev.* **2016**, *116*, 10075.
61. P. Bharmoria, H. Bildirir, K. Moth-Poulsen, *Chem. Soc. Rev.* **2020**, *49*, 6529.
62. M. Uji, T. J. B. Zahringer, C. Kerzig, N. Yanai, *Angew. Chem., Int. Ed.* **2023**, *135*, e202301506.
63. L. Zeng, L. Huang, J. Han, G. Han, *Acc. Chem. Res.* **2022**, *55*, 2604.
64. Y. Niihori, T. Kosaka, Y. Negishi, *Mater. Horiz.* **2024**, *11*, 2304.
65. T. Schloemer, P. Narayanan, Q. Zhou, E. Belliveau, M. Seitz, D. N. Congreve, *ACS Nano* **2023**, *17*, 3259.
66. C. Gao, W. W. H. Wong, Z. S. Qin, S. C. Lo, E. B. Namdas, H. L. Dong, W. P. Hu, *Adv. Mater.* **2021**, *33*, 2100704.
67. A. L. Efros, M. Rosen, M. Kuno, M. Nirmal, D. J. Norris, M. Bawendi, *Phys. Rev. B* **1996**, *54*, 4843.
68. J. Kim, C. Y. Wong, G. D. Scholes, *Acc. Chem. Res.* **2009**, *42*, 1037.
69. M. Korkusinski, O. Voznyy, P. Hawrylak, *Phys. Rev. B* **2010**, *82*, 245304.
70. H. Zhong, M. Nagy, M. Jones, G. D. Scholes, *J. Phys. Chem. C* **2009**, *113*, 10465.
71. J. M. An, A. Franceschetti, A. Zunger, *Nano Lett.* **2007**, *7*, 2129.
72. X. Luo, Y. Han, Z. Chen, Y. Li, G. Liang, X. Liu, T. Ding, C. Nie, M. Wang, F. N. Castellano, K. Wu, *Nat. Commun.* **2020**, *11*, 28.
73. V. Gray, P. Xia, Z. Huang, E. Moses, A. Fast, D. A. Fishman, V. I. Vullev, M. Abrahamsson, K. Moth-Poulsen, M. Lee Tang, *Chem. Sci.* **2017**, *8*, 5488.
74. K. Okumura, N. Yanai, N. Kimizuka, *Chem. Lett.* **2019**, *48*, 1347.
75. S. He, X. Luo, X. Liu, Y. Li, K. Wu, *J. Phys. Chem. Lett.* **2019**, *10*, 5036.
76. L. L. Hou, A. Olesund, S. Thurakkal, X. Y. Zhang, B. Albinsson, *Adv. Funct. Mater.* **2021**, *31*, 2106198.
77. M. Koharagi, N. Harada, K. Okumura, J. Miyano, S. Hisamitsu, N. Kimizuka, N. Yanai, *Nanoscale* **2021**, *13*, 19890.
78. S. He, Y. Han, J. Guo, K. Wu, *J. Phys. Chem. Lett.* **2022**, *13*, 1713.
79. X. Lin, Z. Chen, Y. Han, C. Nie, P. Xia, S. He, J. Li, K. Wu, *ACS Energy Lett.* **2022**, *7*, 914.
80. B. Tang, Q. Wei, S. Wang, H. Liu, N. Mou, Q. Liu, Y. Wu, A. S. Portniagin, S. V. Kershaw, X. Gao, M. Li, A. L. Rogach, *Small* **2024**, *20*, e2311639.
81. Z. Huang, X. Li, M. Mahboub, K. M. Hanson, V. M. Nichols, H. Le, M. L. Tang, C. J. Bardeen, *Nano Lett.* **2015**, *15*, 5552.
82. Z. Huang, X. Li, B. D. Yip, J. M. Rubalcava, C. J. Bardeen, M. L. Tang, *Chem. Mater.* **2015**, *27*, 7503.
83. K. Okumura, K. Mase, N. Yanai, N. Kimizuka, *Chemistry* **2016**, *22*, 7721.
84. X. Li, Z. Huang, R. Zavala, M. L. Tang, *J. Phys. Chem. Lett.* **2016**, *7*, 1955.
85. X. Li, A. Fast, Z. Huang, D. A. Fishman, M. L. Tang, *Angew. Chem., Int. Ed.* **2017**, *56*, 5598.
86. K. Mase, K. Okumura, N. Yanai, N. Kimizuka, *Chem. Commun.* **2017**, *53*, 8261.
87. P. Xia, Z. Huang, X. Li, J. J. Romero, V. I. Vullev, G. S. Pau, M. L. Tang, *Chem. Commun.* **2017**, *53*, 1241.
88. Z. Huang, P. Xia, N. Megerdich, D. A. Fishman, V. I. Vullev, M. L. Tang, *ACS Photonics* **2018**, *5*, 3089.
89. S. Amemori, R. K. Gupta, M. L. Bohm, J. Xiao, U. Huynh, T. Oyama, K. Kaneko, A. Rao, N. Yanai, N. Kimizuka, *Dalton Trans.* **2018**, *47*, 8590.
90. Y. Han, S. He, X. Luo, Y. Li, Z. Chen, W. Kang, X. Wang, K. Wu, *J. Am. Chem. Soc.* **2019**, *141*, 13033.

91. Z. Xu, T. Jin, Y. Huang, K. Mulla, F. A. Evangelista, E. Egap, T. Lian, *Chem. Sci.* **2019**, *10*, 6120.
92. B. Shan, T. T. Li, M. K. Brennaman, A. Nayak, L. Wu, T. J. Meyer, *J. Am. Chem. Soc.* **2019**, *141*, 463.
93. X. Luo, G. Liang, Y. Han, Y. Li, T. Ding, S. He, X. Liu, K. Wu, *J. Am. Chem. Soc.* **2020**, *142*, 11270.
94. R. Lai, Y. Sang, Y. Zhao, K. Wu, *J. Am. Chem. Soc.* **2020**, *142*, 19825.
95. E. M. Rigsby, T. Miyashita, P. Jaimes, D. A. Fishman, M. L. Tang, *J. Chem. Phys.* **2020**, *153*, 114702.
96. R. Lai, K. Wu, *J. Chem. Phys.* **2020**, *153*, 114701.
97. J. De Roo, Z. Huang, N. J. Schuster, L. S. Hamachi, D. N. Congreve, Z. Xu, P. Xia, D. A. Fishman, T. Lian, J. S. Owen, M. L. Tang, *Chem. Mater.* **2020**, *32*, 1461.
98. A. Ronchi, C. Capitani, V. Pinchetti, G. Gariano, M. L. Zaffalon, F. Meinardi, S. Brovelli, A. Monguzzi, *Adv. Mater.* **2020**, *32*, e2002953.
99. S. He, R. Lai, Q. Jiang, Y. Han, X. Luo, Y. Tian, X. Liu, K. Wu, *Angew. Chem., Int. Ed.* **2020**, *59*, 17726.
100. Z. Huang, Z. Xu, T. Huang, V. Gray, K. Moth-Poulsen, T. Lian, M. L. Tang, *J. Am. Chem. Soc.* **2020**, *142*, 17581.
101. Z. A. VanOrman, A. S. Bieber, S. Wiegold, L. Nienhaus, *Chem. Mater.* **2020**, *32*, 4734.
102. Z. A. VanOrman, C. R. Conti, G. F. Strouse, L. Nienhaus, *Chem. Mater.* **2020**, *33*, 452.
103. P. Xia, J. Schwan, T. W. Dugger, L. Mangolini, M. L. Tang, *Adv. Opt. Mater.* **2021**, *9*, 2100453.
104. E. M. Rigsby, T. Miyashita, D. A. Fishman, S. T. Roberts, M. L. Tang, *RSC Adv.* **2021**, *11*, 31042.
105. C. J. Imperiale, P. B. Green, M. Hasham, M. W. B. Wilson, *Chem. Sci.* **2021**, *12*, 14111.
106. T. Miyashita, P. Jaimes, T. Lian, M. L. Tang, Z. Xu, *J. Phys. Chem. Lett.* **2022**, *13*, 3002.
107. P. Jaimes, T. Miyashita, T. Qiao, K. Wang, M. L. Tang, *J. Phys. Chem. C* **2023**, *127*, 1752.
108. M. Wu, D. N. Congreve, M. W. B. Wilson, J. Jean, N. Geva, M. Welborn, T. Van Voorhis, V. Bulović, M. G. Bawendi, M. A. Baldo, *Nat. Photonics* **2015**, *10*, 31.
109. Z. Huang, D. E. Simpson, M. Mahboub, X. Li, M. L. Tang, *Chem. Sci.* **2016**, *7*, 4101.
110. M. Mahboub, Z. Huang, M. L. Tang, *Nano Lett.* **2016**, *16*, 7169.
111. M. Mahboub, H. Maghsoudiganjeh, A. M. Pham, Z. Huang, M. L. Tang, *Adv. Funct. Mater.* **2016**, *26*, 6091.
112. M. Wu, J. Jean, V. Bulović, M. A. Baldo, *Appl. Phys. Lett.* **2017**, *110*, 211101.
113. L. Nienhaus, M. Wu, N. Geva, J. J. Shepherd, M. W. B. Wilson, V. Bulovic, T. Van Voorhis, M. A. Baldo, M. G. Bawendi, *ACS Nano* **2017**, *11*, 7848.
114. Z. Huang, Z. Xu, M. Mahboub, X. Li, J. W. Taylor, W. H. Harman, T. Lian, M. L. Tang, *Angew. Chem., Int. Ed.* **2017**, *56*, 16583.
115. M. Mahboub, P. Xia, J. Van Baren, X. Li, C. H. Lui, M. L. Tang, *ACS Energy Lett.* **2018**, *3*, 767.
116. Z. Huang, Z. Xu, M. Mahboub, Z. Liang, P. Jaimes, P. Xia, K. R. Graham, M. L. Tang, T. Lian, *J. Am. Chem. Soc.* **2019**, *141*, 9769.
117. L. Nienhaus, J.-P. Correa-Baena, S. Wiegold, M. Einzinger, T.-A. Lin, K. E. Shulenberger, N. D. Klein, M. Wu, V. Bulović, T. Buonassisi, M. A. Baldo, M. G. Bawendi, *ACS Energy Lett.* **2019**, *4*, 888.
118. N. Nishimura, J. R. Allardice, J. Xiao, Q. Gu, V. Gray, A. Rao, *Chem. Sci.* **2019**, *10*, 4750.
119. S. Wiegold, A. S. Bieber, Z. A. VanOrman, L. Daley, M. Leger, J.-P. Correa-Baena, L. Nienhaus, *Matter* **2019**, *1*, 705.
120. Z. Xu, Z. Huang, C. Li, T. Huang, F. A. Evangelista, M. L. Tang, T. Lian, *ACS Appl. Mater. Interfaces* **2020**, *12*, 36558.
121. E. M. Gholizadeh, S. K. K. Prasad, Z. L. Teh, T. Ishwara, S. Norman, A. J. Petty, J. H. Cole, S. Cheong, R. D. Tilley, J. E. Anthony, S. Huang, T. W. Schmidt, *Nat. Photonics* **2020**, *14*, 585.
122. M. Wu, T. A. Lin, J. O. Tjepelt, V. Bulovic, M. A. Baldo, *Nano Lett.* **2021**, *21*, 1011.
123. N. Tripathi, M. Ando, T. Akai, K. Kamada, *ACS Appl. Nano Mater.* **2021**, *4*, 9680.
124. W. Liang, C. Nie, J. Du, Y. Han, G. Zhao, F. Yang, G. Liang, K. Wu, *Nat. Photonics* **2023**, *17*, 346.
125. L.-H. Jiang, X. Miao, M.-Y. Zhang, J.-Y. Li, L. Zeng, W. Hu, L. Huang, D.-W. Pang, *J. Am. Chem. Soc.* **2024**, *146*, 10785.
126. S. He, Y. Han, J. Guo, K. Wu, *J. Phys. Chem. Lett.* **2021**, *12*, 8598.
127. J. Isokuortti, S. R. Allu, A. Efimov, E. Vuorimaa-Laukkanen, N. V. Tkachenko, S. A. Vinogradov, T. Laaksonen, N. A. Durandin, *J. Phys. Chem. Lett.* **2020**, *11*, 318.
128. A. D. McNaught, A. Wilkinson, P. International Union of, C. Applied, *Compendium of Chemical Terminology: IUPAC Recommendations*, 2nd ed., Blackwell Science, Oxford **1997**.
129. Y. Zhou, F. N. Castellano, T. W. Schmidt, K. Hanson, *ACS Energy Lett.* **2020**, *5*, 2322.
130. D. Beery, J. P. Wheeler, A. Arcidiacono, K. Hanson, *ACS Appl. Energy Mater.* **2019**, *3*, 29.
131. V. Gray, D. Dzebo, M. Abrahamsson, B. Albinsson, K. Moth-Poulsen, *Phys. Chem. Chem. Phys.* **2014**, *16*, 10345.
132. T. Dilbeck, K. Hanson, *J. Phys. Chem. Lett.* **2018**, *9*, 5810.
133. M. Majek, U. Faltermeier, B. Dick, R. Perez-Ruiz, A. Jacobi von Wangelin, *Chem. Eur J.* **2015**, *21*, 15496.
134. D. G. Bossanyi, Y. Sasaki, S. Q. Wang, D. Chekulaev, N. Kimizuka, N. Yanai, J. Clark, *J. Am. Chem. Soc. Au* **2021**, *1*, 2188.
135. S. Hoseinkhani, R. Tubino, F. Meinardi, A. Monguzzi, *Phys. Chem. Chem. Phys.* **2015**, *17*, 4020.
136. W. J. Sun, A. Ronchi, T. H. Zhao, J. L. Han, A. Monguzzi, P. F. Duan, *J. Mater. Chem. C* **2021**, *9*, 14201.
137. Y. Y. Cheng, B. Fockel, T. Khoury, R. G. C. R. Clady, M. J. Y. Tayebjee, N. J. Ekins-Daukes, M. J. Crossley, T. W. Schmidt, *J. Phys. Chem. Lett.* **2010**, *1*, 1795.
138. V. Gray, D. Dzebo, A. Lundin, J. Alborzpour, M. Abrahamsson, B. Albinsson, K. Moth-Poulsen, *J. Mater. Chem. C* **2015**, *3*, 11111.
139. A. Olesund, V. Gray, J. Martensson, B. Albinsson, *J. Am. Chem. Soc.* **2021**, *143*, 5745.
140. X. Luo, R. C. Lai, Y. L. Li, Y. Y. Han, G. J. Liang, X. Liu, T. Ding, J. H. Wang, K. F. Wu, *J. Am. Chem. Soc.* **2019**, *141*, 4186.
141. Z. Y. Huang, M. L. Tang, *J. Am. Chem. Soc.* **2017**, *139*, 9412.
142. Y. Y. Han, S. He, K. F. Wu, *ACS Energy Lett.* **2021**, *6*, 3151.
143. V. Gray, J. R. Allardice, Z. Zhang, A. Rao, *Chem. Phys. Rev.* **2021**, *2*, 031305.
144. T. W. Schmidt, F. N. Castellano, *J. Phys. Chem. Lett.* **2014**, *5*, 4062.
145. X. P. Wang, R. Tom, X. Y. Liu, D. N. Congreve, N. Marom, *J. Mater. Chem. C* **2020**, *8*, 10816.
146. M. Montalti, A. Credi, L. Prodi, M. T. Gandolfi, *Handbook of Photochemistry*, 3rd ed., Taylor and Francis, Boca Raton **2006**.
147. L. Huang, E. Kakadiaris, T. Vaneckova, K. Huang, M. Vaculovicova, G. Han, *Biomaterials* **2019**, *201*, 77.
148. A. L. Efros, M. Rosen, *Annu. Rev. Mater. Sci.* **2000**, *30*, 475.
149. A. Monguzzi, J. Mezyk, F. Scotognella, R. Tubino, F. Meinardi, *Phys. Rev. B* **2008**, *78*, 195112.
150. A. Haefele, J. Blumhoff, R. S. Khnazyer, F. N. Castellano, *J. Phys. Chem. Lett.* **2012**, *3*, 299.
151. W. W. Yu, L. H. Qu, W. Z. Guo, X. G. Peng, *Chem. Mater.* **2003**, *15*, 2854.
152. L. Cademartiri, E. Montanari, G. Calestani, A. Migliori, A. Guagliardi, G. A. Ozin, *J. Am. Chem. Soc.* **2006**, *128*, 10337.
153. F. Edhborg, A. Olesund, B. Albinsson, *Photochem. Photobiol. Sci.* **2022**, *21*, 1143.
154. A. Olesund, J. Johnsson, F. Edhborg, S. Ghasemi, K. Moth-Poulsen, B. Albinsson, *J. Am. Chem. Soc.* **2022**, *144*, 3706.
155. X. G. Peng, *Adv. Mater.* **2003**, *15*, 459.
156. C. B. Murray, S. H. Sun, W. Gaschler, H. Doyle, T. A. Betley, C. R. Kagan, *IBM J. Res. Dev.* **2001**, *45*, 47.
157. W. A. Tisdale, X. Y. Zhu, *Proc. Natl. Acad. Sci. U.S.A.* **2011**, *108*, 965.
158. H. Zhu, N. Song, T. Lian, *J. Am. Chem. Soc.* **2010**, *132*, 15038.
159. H. Zhu, Y. Yang, K. Hyeon-Deuk, M. Califano, N. Song, Y. Wang, W. Zhang, O. V. Prezhdo, T. Lian, *Nano Lett.* **2014**, *14*, 1263.

160. A. Heuer-Jungemann, N. Feliu, I. Bakaimi, M. Hamaly, A. Alkilany, I. Chakraborty, A. Masood, M. F. Casula, A. Kostopoulou, E. Oh, K. Susumu, M. H. Stewart, I. L. Medintz, E. Stratakis, W. J. Parak, A. G. Kanaras, *Chem. Rev.* **2019**, *119*, 4819.
161. M. A. Boles, D. S. Ling, T. Hyeon, D. V. Talapin, *Nat. Mater.* **2016**, *15*, 364.
162. M. A. El-Sayed, *Acc. Chem. Res.* **2004**, *37*, 326.
163. Z. A. Peng, X. G. Peng, *J. Am. Chem. Soc.* **2001**, *123*, 183.
164. S. G. Kwon, T. Hyeon, *Small* **2011**, *7*, 2685.
165. P. Reiss, M. Protiere, L. Li, *Small* **2009**, *5*, 154.
166. B. T. Ji, S. Koley, I. Slobodkin, S. Remennik, U. Banin, *Nano Lett.* **2020**, *20*, 2387.
167. J. T. Mulder, N. Kirkwood, L. De Trizio, C. Li, S. Bals, L. Manna, A. J. Houtepen, *ACS Appl. Nano Mater.* **2020**, *3*, 3859.
168. G. Konstantatos, *Colloidal Quantum Dot Optoelectronics and Photovoltaics*, Cambridge University Press, New York **2013**.
169. J. Zhang, H. Kouno, N. Yanai, D. Eguchi, T. Nakagawa, N. Kimizuka, T. Teranishi, M. Sakamoto, *ACS Photonics* **2020**, *7*, 1876.
170. G. Zhao, Z. Chen, K. Xiong, G. Liang, J. Zhang, K. Wu, *Nanoscale* **2021**, *13*, 1303.
171. M. T. Frederick, V. A. Amin, N. K. Swenson, A. Y. Ho, E. A. Weiss, *Nano Lett.* **2013**, *13*, 287.
172. C. Jia, X. Guo, *Chem. Soc. Rev.* **2013**, *42*, 5642.
173. C. K. Yong, A. J. Musser, S. L. Bayliss, S. Lukman, H. Tamura, O. Bubnova, R. K. Hallani, A. Meneau, R. Resel, M. Maruyama, S. Hotta, L. M. Herz, D. Beljonne, J. E. Anthony, J. Clark, H. Sirringhaus, *Nat. Commun.* **2017**, *8*, 15953.
174. R. R. Islangulov, J. Lott, C. Weder, F. N. Castellano, *J. Am. Chem. Soc.* **2007**, *129*, 12652.
175. J. Alves, J. L. Feng, L. Nienhaus, T. W. Schmidt, *J. Mater. Chem. C* **2022**, *10*, 7783.
176. R. Vadrucchi, C. Weder, Y. C. Simon, *Mater. Horiz.* **2015**, *2*, 120.
177. P. F. Duan, N. Yanai, N. Kimizuka, *J. Am. Chem. Soc.* **2013**, *135*, 19056.
178. K. Sripathy, R. W. MacQueen, J. R. Peterson, Y. Y. Cheng, M. Dvorak, D. R. McCamey, N. D. Treat, N. Stingelin, T. W. Schmidt, *J. Mater. Chem. C* **2015**, *3*, 616.
179. T. Ogawa, N. Yanai, A. Monguzzi, N. Kimizuka, *Sci. Rep.* **2015**, *5*, 10882.
180. Y. Jiang, C. Wang, C. R. Rogers, M. S. Kodaimati, E. A. Weiss, *Nat. Chem.* **2019**, *11*, 1034.
181. Y. Jiang, M. Yang, Y. Wu, R. Lopez-Arteaga, C. R. Rogers, E. A. Weiss, *Chem Catal.* **2021**, *1*, 106.
182. J. S. Lissau, D. Nauroozi, M.-P. Santoni, S. Ott, J. M. Gardner, A. Morandeira, *J. Phys. Chem. C* **2013**, *117*, 14493.
183. S. P. Hill, K. Hanson, *J. Am. Chem. Soc.* **2017**, *139*, 10988.
184. Y. Y. Cheng, A. Nattestad, T. F. Schulze, R. W. MacQueen, B. Fackel, K. Lips, G. G. Wallace, T. Khoury, M. J. Crossley, T. W. Schmidt, *Chem. Sci.* **2016**, *7*, 559.
185. S. P. Hill, T. Dilbeck, E. Baduell, K. Hanson, *ACS Energy Lett.* **2016**, *1*, 3.

AUTHOR BIOGRAPHIES



Kezhou Chen obtained Bachelor degree from Chongqing University (2021) and now is a PhD student at the Molecular Photonics Lab in the School of Precision Instrument and Opto-electronic Engineering, Tianjin University. His research focuses on light-induced energy transfer process, photo-responsive materials and their applications in encryption and display.



Qingxin Luan obtained Bachelor degree from University of Jinan (2022) and now is a Master student at the Molecular Photonics Lab in the School of Precision Instrument and Opto-Electronics Engineering, Tianjin University. His research interests mainly focus on triplet-triplet annihilation photon upconversion and photochemical reactions based on quantum dots.



Bo Albinsson has MSc and PhD (1993) from Chalmers University of Technology and was post-doctoral fellow at the University of Colorado before returning to Sweden as an assistant professor funded by the Swedish research council in 1995. In 2003 he became full professor of Physical Chemistry at Chalmers and has since then been leading a medium size research group. In the Albinsson research group the focus is on photo-induced processes ranging from mechanistic studies of energy and electron transfer reactions with relevance for solar energy research to novel functionalized nanostructures based on DNA nanotechnology. During the last 10 years the group has concentrated their efforts on studies of photon up and down conversion based on triplet-triplet annihilation and singlet fission, respectively. Advanced laser-based time-resolved spectroscopic techniques combined with traditional optical spectroscopy and theoretical methods are the main tools. About 20 PhD students have graduated from the group, many of which today either hold prominent positions in the industry or embarked on successful careers in academia. More than 170 papers have been published almost exclusively in highly ranked journals. Bo Albinsson was Head of the Department/Division of Chemistry and Biochemistry (2006–2014) and Director of the Nano Excellence Initiative at Chalmers between 2015 and 2021. Bo Albinsson is a Fellow of the Royal Swedish Academy of Sciences (KVA), and he is often recruited as evaluator and reviewer both nationally and internationally.



Tiegeng Liu has MSc and PhD (1999) Degree in Engineering from Tianjin University. He is now the chair professor of national core disciplines, the School of Precision Instrument and Opto-Electronics Engineering, Tianjin University. Tiegeng Liu is the chief scientist of the National Basic Research Program of China (973 Program), and the specialist privileged by special government allowances of the State Council in China. His research engaged in optical fiber sensing theory and technology, photoelectric detection technology, and fusion perception of photoelectric information. He is now an executive director of China Instrument and Control

Society (CIS) and the president of the Opto-mechatronics Technology and System Integration Branch, the executive director of Chinese Optical Society (COS) and the first deputy director of Optoelectronic Technology Professional Committee. He was the former director of Key Laboratory of Optoelectronic Information Technology, Ministry of Education. So far, Tiegeng Liu has owned 126 national invention patents and 10 international patents. He has published more than 395 papers in academic journals and international conferences, and has fostered 18 post-docs, 76 doctors and more than 100 masters.



Lili Hou obtained her Master degree from Tianjin University, China, and PhD degree from Stratingh Institute for Chemistry (2023), University of Groningen, the Netherlands. After that she worked as a post-doc at the University of Strasbourg, France, and then worked as a researcher at the Department of Chemistry and Chemical Engineering, Chalmers University of Technology, Sweden. In 2021,

she became a Full-Professor in Optical Engineering at Tianjin University, and in 2022 She became an affiliated docent-Professor in Physical Chemistry at Chalmers University of Technology. Lili Hou is now the young chief scientist of National Key Research and Development Project of China. Her research interests include photon upconversion, light-induced energy/electron transfer processes, advanced light-responsive materials and optoelectronics devices. As a Principal Investigator, she leads the Molecular Photonics Lab at Tianjin University. So far, She has published more than 30 papers almost exclusively in highly ranked journals including *Nature Nanotechnology*, *JACS*, *Nature Communication*, etc.

How to cite this article: K. Chen, Q. Luan, T. Liu, B. Albinsson, L. Hou, *Responsive Mater.* **2025**, *3*, e20240030. <https://doi.org/10.1002/rpm.20240030>